Dendrites as climbing dislocations in ceramic electrolytes: initiation of growth

S. S. Shishvan[a,b], N.A. Fleck[b], R.M. McMeeking[c,d,e] and V.S. Deshpande[b*]

[a] *Department of Structural Engineering, University of Tabriz, Tabriz, Iran*

[b] *Department of Engineering, University of Cambridge, Cambridge CB2 1PZ, UK*

[c] *Department of Mechanical Engineering & Materials Department, University of California, Santa Barbara CA 93106, USA*

[d] *School of Engineering, Aberdeen University, King's College, Aberdeen AB24 3UE, UK*

[e] *INM – Leibniz Institute for New Materials, Campus D2 2, 66123 Saarbrücken, Germany*

Abstract

We idealise dendrite growth in a ceramic electrolyte by climb of a thick edge dislocation. Growth of the dendrite occurs at constant chemical potential of Li^+ at the dendrite tip: the free-energy to fracture and wedge open the electrolyte is provided by the flux of Li^+ from the electrolyte into the dendrite tip. This free-energy is dependent on the Li^+ overpotential at the dendrite tip and is thereby related to the imposed charging current density. The predicted critical current density agrees with measurements for Li/LLZO/Li symmetric cells: the critical current density decreases with increasing initial length of the dendrite and with increasing electrode/electrolyte interfacial ionic resistance. The simulations also reveal that a void on the cathode/electrolyte interface locally enhances the Li^+ overpotential and significantly reduces the critical current density for the initiation of dendrite growth.

Keywords: Ceramic separator, solid-state battery, Lithium dendrite, free-energy.

*Corresponding author. E-mail address: vsd@eng.cam.ac.uk

1. Introduction

Lithium-ion batteries comprising Lithium (Li) metal anodes, ceramic cathodes (such as NMC), and ceramic electrolytes (such as the Li-stuffed garnet $Li_7La_3Zr_2O_{12}$, (LLZO)) have high specific energy densities [1, 2], a high Li^+ ion conductivity, and can be processed to ensure relatively low interfacial ionic resistance across the electrolyte/Li interface. However, they can short-circuit by the growth of Li-filled fissures, or 'dendrites' across the electrolyte. These dendrites differ from the mossy growth [3], needle-like protrusions or globular structures [4, 5] that form in liquid electrolytes due to surface instabilities [6, 7].

Symmetric Li/Li cells containing LLZO electrolytes also short circuit by dendrite formation [8-11]. The critical current density i_{CCD} is the minimum charging current to short circuit the cell; it increases with increasing grain size of electrolyte [9] and with decreasing electrolyte/electrode ionic resistance Z [8]. The dendrites may comprise parallel-sided sheets filled with Li [12, 13] and resemble edge dislocations of large Burgers vector (approximately 30 nm). Similarly, Na dendrites in Na^+/beta-alumina systems also resemble edge dislocations [14] although high-resolution imaging of dendrites in solid electrolytes has to-date not been reported in the literature.

While electrode fracture has been widely explored [15, 16], the modelling of dendrites in ceramic electrolytes has been restricted to idealising them as pressurised cracks [17-20]: crack propagation is driven by pressurised Li within the crack generated by the electric overpotential across the crack flanks [19]. However, the pressurised crack model implies unrealistically low values of fracture toughness of the electrolyte in order to predict the low measured values of i_{CCD} [17]. Moreover, the model assumes that the pressurised Li does not leak from crack mouth into the adjacent Li electrode.

Here, we present an alternative mechanism for the initiation of dendrite growth by treating dendrites as thick edge-dislocations with dendrite growth occurring by fracture of the electrolyte at the dendrite tip at constant chemical potential of Li^+. A list of the mathematical symbols used in the analysis is provided in Table 1.

2. Dendrites as climbing edge dislocations

Dendrite penetration of Li into ceramic electrolytes occurs from the Li metal cathode (defined as the electrode at which the reduction reaction occurs). The available data [12-14] suggest that mode, as sketched in Fig. 1a, is reminiscent of a climbing edge dislocation with large Burgers vector $b = 10 - 100$ nm, such that the flanks of the fractured electrolyte are parallel-sided and filled by Li of thickness b. *We propose that this is one viable mode of Li penetration since it satisfies all the required electro-chemo-mechanical governing laws*; other competing modes of Li penetration may exist but have not (yet) been identified.

Consider a pre-existing dendrite of length a_0 and Burgers vector of magnitde b emanating from the cathodic interface, see Fig. 1a. We focus on the required conditions for dendrite growth by the simultaneous cracking of the electrolyte and the deposition of Li into the dendrite tip by Li^+ flux from the electrolyte during the plating phase. The analysis assumes:

(i) an electroneutral electrolyte [17-19] of uniform and constant concentration of Li, and

(ii) a vanishing molar volume Ω_e of Li within the electrolyte [19], such that the Li lies within a ceramic skeleton that remains rigid upon removal/addition of a Li atom.

These assumptions significantly reduce the complexity of the governing equations and allow for all the required material and interfacial properties for Li/LLZO/Li symmetric cells to be gleaned from experimental measurements or first principle calculations from the literature.

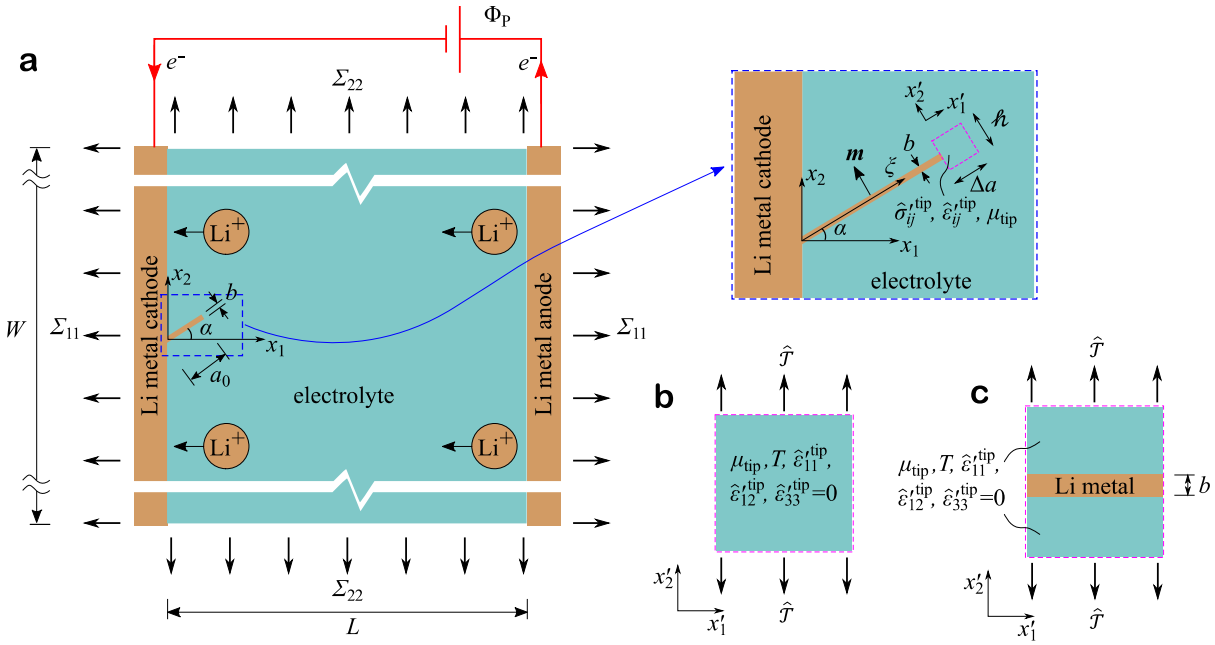

Figure 1: (a) Sketch of a symmetric cell comprising a single ion-conductor ceramic electrolyte of thickness L and width W and Li electrodes covering the electrolyte. The electrolyte is subjected to uniform remote stresses Σ_{11} and Σ_{22}. A dendrite of length a_0 and Burgers vector b emanates at an angle α from the cathode with ξ an intrinsic co-ordinate measured along the dendrite from its root. We fix the global co-ordinate system (x_1, x_2) at the root of the dendrite and also define a local co-ordinate system (x_1', x_2') aligned with the dendrite. The stress and strain state of the electrolyte directly ahead of the dendrite (using the x_i' co-ordinate system) are $\hat{\sigma}_{ij}'^{\,\text{tip}}$ and $\hat{\varepsilon}_{ij}'^{\,\text{tip}}$, respectively, with μ_{tip} denoting the chemical potential Li^+ in the electrolyte at that location. (b) A sketch of a system representing the electrolyte directly ahead of the dendrite (see inset in (a)). The system is maintained at a constant chemical potential μ_{tip} of Li^+ and the stresses and strains held fixed are labelled. (c) A sketch of the state of the system after fracture with the dendrite propagating through the system and sandwiched between the electrolyte.

Table 1 A summary of the parameters of the model.

Symbol	Brief description
A_{m}	The Helmholtz free-energy of the Li metal electrode
a_0	Dendrite length
B	Out-of-plane thickness of electrolyte
b	Burgers vector magnitude
b_{CCD}	Burgers vector magnitude that minimizes i_{min}
E_{Li}	Young's modulus of the Li metal electrode
E_i	The electric field
$\mathcal{E}$	Permittivity of electrolyte
F	Faraday constant
f_{climb}	The climb component of the Peach-Koehler force
f_i	Driving force for the flux of Li^+
G	Shear modulus of the electrolyte
$\mathcal{G}_{\mathrm{e}}$	The Gibbs free-energy of the electrolyte
$\mathcal{G}_{\mathrm{m}}$	The Gibbs free-energy of the Li metal electrode
h_i	The molar flux of Li^+ in the electroneutral electrolyte
H_{m}	The enthalpy of the Li metal electrode
h_{v}	The molar enthalpy of formation of vacant sites in the Li metal electrode
$\hbar$	The arbitrary height of a system defined at the dendrite tip
i_{CCD}	The critical current required to initiate dendrite growth in the electrolyte
i_{min}	The minimum current required to initiate dendrite growth in the electrolyte for a given b
j	The areal current density of Li^+ flux between the electrode and electrolyte (positive from electrode to electrolyte)
j_0	The exchange current density
$\bar{j}_0$	The exchange current density at zero pressure
j_∞	A nominal current density (positive for current in the positive x_1 −direction)
j_i	Current of the Li^+ ions in the electrolyte in the global co-ordinate system x_i
k_{tip}	The overpotential concentration factor at the dendrite tip
k_η	The overpotential concentration factor
L	Thickness of electrolyte
$\mathcal{L}_{\mathrm{tip}}$	Free-energy of the system defined in the electrolyte at the dendrite tip
ℓ	The void size on the cathodic interface
m	The mobility of Li^+ in the electrolyte
m_i	A unit vector perpendicular to the dendrite
N	Moles of Li^+ that flux into the dendrite due to dendrite growth by a distance Δa
N_{Li^+}	Moles of Li^+ in the system defined in the electrolyte ahead of the dendrite tip
$N_{\mathrm{L}}^{\mathrm{e}}$	Moles of Li^+ sites in the electrolyte
$N_{\mathrm{Li}^+}^{\mathrm{e}}$	The number of moles of Li^+ ions within the electrolyte
$N_{\mathrm{L}}^{\mathrm{m}}$	Moles of lattice sites in the Li metal
$N_{\mathrm{Li}}^{\mathrm{m}}$	Moles of Li atoms in the Li metal electrode
N_{v}	Moles of vacant lattice sites in the Li metal electrode
n_j	The unit outward normal to the electrolyte
$p(\xi)$	The pressure in the electrolyte at location ξ along the dendrite
p_{m}	Pressure in the Li metal electrode

$\hat{p}_{\mathrm{tip}}$	The dendrite tip pressure associated with the image field
R	Gas constant
S_{m}	Entropy of the Li metal electrode
s_{tip}	The specific entropy of the system defined in the electrolyte at the dendrite tip
T	Temperature
T_i^0	The applied external tractions
$\hat{\mathcal{T}}$	The traction due to the image field on a system at the dendrite tip
U_{m}	The internal energy of the Li metal electrode
$\mathcal{U}$	The open circuit potential
u_i	The displacement field in the global co-ordinate system x_i
W	Width of electrolyte
x_i	Global co-ordinate system
x_i'	Local co-ordinate system aligned with the dendrite
Z	The interfacial ionic resistance
α	Angle of the dendrite emanating from the cathode in a symmetric cell
β	The Butler-Volmer symmetry factor
$\gamma_{\mathrm{e/Li}}$	Energy per unit area of the electrolyte/Li metal interface
ε_{ij}	Strain in the global co-ordinate system x_i
$\hat{\varepsilon}_{ij}'^{\,\mathrm{tip}}$	Strain state of the electrolyte directly ahead of the dendrite (using the x_i' co-ordinate system)
Δa	An infinitesimal propagation distance of the dendrite
δ_{ij}	Kronecker delta
η	The overpotential
$\eta(\xi)$	The overpotential at location ξ along the dendrite
η_{c}	The critical dendrite-tip overpotential
η_{tip}	The overpotential of the electrolyte at the dendrite tip
θ_{e}^0	Occupancy of Li^+sites within the electrolyte
θ_{m}	Occupancy of the Li atoms in the Li metal electrode (labelled as θ_{m}^0 at zero pressure)
$\theta_{\mathrm{m}}(\xi)$	Occupancy of Li sites at location ξ along the dendrite
θ_{tip}	Occupancy of lattice sites within the metal phase at the dendrite tip
θ_{v}	Occupancy of vacant lattice sites in the Li metal electrode (labelled as θ_{v}^0 at zero pressure)
κ	Ionic conductivity of the electrolyte
$\mu_{\mathrm{Li^+}}^{\mathrm{e}}$	Chemical potential of the Li^+ ions within the electrolyte
μ_{e}^0	The reference molar enthalpy of the Li^+ ions in the electrolyte
μ_{m}^0	The reference molar enthalpy of the Li atoms
$\mu_{\mathrm{el^-}}^{\mathrm{m}}$	The chemical potential of the electrons (the Fermi level) in the Li electrode
$\mu_{\mathrm{Li}}^{\mathrm{m}}$	The chemical potential of the Li atoms in the Li metal electrode
$\mu_{\mathrm{Li^+}}^{\mathrm{m}}$	The chemical potential of the Li^+ ions in the electroneutral metal electrode
μ_{tip}	The chemical potential of Li^+ ions at the dendrite tip
ν	Poisson's ratio of the electrolyte
ξ	An intrinsic co-ordinate measured along the dendrite from its root
ρ_{m}	The theoretical molar density of Li
ρ_{f}	The density of free-charge
Σ_{ij}	Remote stresses
σ_{ij}	Stress in the global co-ordinate system x_i
σ_{ij}^{M}	Maxwell stresses

$\tilde{\sigma}_{ij}$	Singular stress field of an edge dislocation in an infinite medium
$\hat{\sigma}_{ij}$	Image stress field of an edge dislocation in a medium
$\hat{\sigma}_{ij}^{\text{tip}}$	The components of the image stresses at the dendrite tip in the global co-ordinate system
$\hat{\sigma}_{ij}^{\prime\,\text{tip}}$	Stress state of the electrolyte directly ahead of the dendrite (using the x_i' co-ordinate system)
Φ_{P}	Applied electrical potential to the anode
ϕ_{A}	The electric potential in the electrolyte at the electrolyte/anode interface
$\phi_{\text{d}}(\xi)$	The electric potential in the electrolyte at location ξ along the dendrite
$\phi \equiv \phi_{\text{e}}$	The electric potential of the electrolyte
ϕ_{m}	The electric potential in the Li metal electrode
ϕ_{tip}	The electric potential of the electrolyte at dendrite tip
Ω	Volume of the Li metal electrode
Ω_{e}	The molar volume of Li within the electrolyte
Ω_{Li}	Molar volume of Li in the electrode
Ω_{v}	Molar volume of the vacant sites in the Li metal electrode

2.1 Chemical potential definitions and equilibrium states

Consider the Li metal electrode (that is maintained to be electrically neutral) comprising N_{L}^{m} moles of lattice sites that are occupied by N_{Li}^{m} moles of Li atoms, where the subscript "L" denotes lattice and the superscript "m" denotes the metallic electrode. The Li atoms have an occupancy $\theta_{\text{m}} \equiv N_{\text{Li}}^{\text{m}}/N_{\text{L}}^{\text{m}}$ and $N_{\text{v}} = N_{\text{L}}^{\text{m}} - N_{\text{Li}}^{\text{m}}$ lattice sites are vacant, with $\theta_{\text{v}} \equiv N_{\text{v}}/N_{\text{L}}^{\text{m}}$ denoting the fraction of these vacant sites. The electrode is subjected to a pressure (positive in compression) p_{m} and electrical potential ϕ_{m}. Let Ω_{Li} denote the molar volume of Li, Ω_{v} denote the molar volume of vacant sites, and $\Omega \equiv (N_{\text{Li}}^{\text{m}}\Omega_{\text{Li}} + N_{\text{v}}\Omega_{\text{v}})$ denote the volume of the system such that $\Omega_{\text{v}} \equiv (\partial\Omega/\partial N_{\text{L}}^{\text{m}})_{N_{\text{Li}}^{\text{m}}}$. Assuming that insertion of a Li atom causes negligible deviatoric straining, the enthalpy of the Li metal electrode is

$$H_{\text{m}} = N_{\text{Li}}^{\text{m}}(\mu_{\text{m}}^{0} + p_{\text{m}}\,\Omega_{\text{Li}}) + N_{\text{v}}(h_{\text{v}} + p_{\text{m}}\Omega_{\text{v}}), \tag{2.1}$$

where h_{v} is the molar enthalpy of formation of vacant sites in Li defined in the usual manner as $h_{\text{v}} \equiv (\partial H_{\text{m}}/\partial N_{\text{L}}^{\text{m}})_{N_{\text{Li}}^{\text{m}}}$ at $p_{\text{m}} = 0$. In (2.1), μ_{m}^{0} is the reference molar enthalpy of the Li atoms that we shall define more precisely below in Eq. (2.4) in the context of the chemical potential of Li. In writing (2.1), we have neglected the contribution from elastic straining: this

contribution is on the order of $N_{\mathrm{Li}}^{\mathrm{m}}\Omega_{\mathrm{Li}}p_{\mathrm{m}}^2/E_{\mathrm{Li}}$ where E_{Li} is the Young's modulus of the Li. This contribution is negligible since $p_{\mathrm{m}} \ll E_{\mathrm{Li}}$.

The internal energy of the system is given by the appropriate Legendre transform of H_{m} as $U_{\mathrm{m}} \equiv H_{\mathrm{m}} - p_{\mathrm{m}}\Omega$, where $\Omega = (\partial H_{\mathrm{m}}/\partial p_{\mathrm{m}})_{S_{\mathrm{m}}}$ at fixed entropy S_{m} of the system. We neglect vibrational entropy and, therefore set the entropy of $N_{\mathrm{Li}}^{\mathrm{m}}$ moles of Li atoms, and N_{v} moles of vacant sites, equal to zero prior to mixing. Then, S_{m} is given in terms of the gas constant R by the entropy of mixing as

$$S_{\mathrm{m}} = -N_{\mathrm{L}}^{\mathrm{m}}\, R[\theta_{\mathrm{m}} \ln \theta_{\mathrm{m}} + (1-\theta_{\mathrm{m}}) \ln(1-\theta_{\mathrm{m}})]\,, \tag{2.2}$$

The Helmholtz free-energy at temperature $T \equiv (\partial U_{\mathrm{m}}/\partial S_{\mathrm{m}}\,)_{\Omega}$ follows as $A_{\mathrm{m}} \equiv U_{\mathrm{m}} - TS_{\mathrm{m}}$, such that

$$A_{\mathrm{m}} = N_{\mathrm{Li}}^{\mathrm{m}}\mu_{\mathrm{m}}^{0} + N_{\mathrm{v}}h_{\mathrm{v}} + N_{\mathrm{L}}^{\mathrm{m}}\, RT[\theta_{\mathrm{m}} \ln \theta_{\mathrm{m}} + (1-\theta_{\mathrm{m}}) \ln(1-\theta_{\mathrm{m}})], \tag{2.3}$$

and Gibbs free-energy of the system is $\mathcal{G}_{\mathrm{m}} \equiv A_{\mathrm{m}} + p_{\mathrm{m}}\Omega$. To calculate the chemical potential of Li, we consider an isobaric-isothermal ensemble (NpT −ensemble) where the only particles in the system are Li atoms (i.e. lattice sites and Li atoms are the two species in the system). The chemical potential of the Li atoms then follows as

$$\mu_{\mathrm{Li}}^{\mathrm{m}} \equiv \left.\frac{\partial \mathcal{G}_{\mathrm{m}}}{\partial N_{\mathrm{Li}}^{\mathrm{m}}}\right|_{N_{\mathrm{L}}^{\mathrm{m}}} = (\mu_{\mathrm{m}}^{0} - h_{\mathrm{v}}) + p_{\mathrm{m}}(\Omega_{\mathrm{Li}} - \Omega_{\mathrm{v}}) + RT\ln\left(\frac{\theta_{\mathrm{m}}}{1-\theta_{\mathrm{m}}}\right). \tag{2.4}$$

We shall assume that the electrode comprising $N_{\mathrm{Li}}^{\mathrm{m}}$ moles of Li atoms is in equilibrium with a vacancy reservoir as the free-surfaces of the electrode can readily generate/annihilate vacancies. Within the context of the NpT −ensemble, the system attains equilibrium with the vacancy reservoir at fixed $N_{\mathrm{Li}}^{\mathrm{m}}$ by changing its volume, here parameterised by $N_{\mathrm{L}}^{\mathrm{m}}$. This implies that at equilibrium

$$\left.\frac{\partial \mathcal{G}_{\mathrm{m}}}{\partial N_{\mathrm{L}}^{\mathrm{m}}}\right|_{N_{\mathrm{Li}}^{\mathrm{m}}} = 0, \tag{2.5}$$

and it follows that the fraction of vacant sites at an applied pressure $p_{\mathrm{m}} = 0$ is $\theta_{\mathrm{v}}^{0} = \exp[-h_{\mathrm{v}}/(RT)]$ while at a non-zero pressure p_{m} we have $\theta_{\mathrm{v}} = \theta_{\mathrm{v}}^{0}\exp[-p_{\mathrm{m}}\Omega_{\mathrm{v}}/(RT)]$. The occupancy of lattice sites by Li atoms is then $\theta_{\mathrm{m}} = 1 - \theta_{\mathrm{v}}$. Note that the enthalpy of formation of vacant sites in Li is $h_{\mathrm{v}} \approx 50$ kJ mol^{-1} [21]; consequently, at room temperature $T = 300$ K, we have $h_{\mathrm{v}}/(RT) \gg 1$ and therefore $\theta_{\mathrm{v}} \ll 1$ and $\theta_{\mathrm{m}} \approx 1$. Using this approximation, it is convenient to express the occupancies of lattice sites by Li atoms as

$$\frac{\theta_{\mathrm{m}}}{1-\theta_{\mathrm{m}}} = \frac{\theta_{\mathrm{m}}^{0}}{1-\theta_{\mathrm{m}}^{0}}\exp\left(\frac{p_{\mathrm{m}}\Omega_{\mathrm{v}}}{RT}\right), \tag{2.6}$$

where

$$\frac{\theta_{\mathrm{m}}^{0}}{1-\theta_{\mathrm{m}}^{0}} = \exp\left(\frac{h_{\mathrm{v}}}{RT}\right). \tag{2.7}$$

Here, $\theta_{\mathrm{m}}^{0} = 1 - \theta_{\mathrm{v}}^{0}$ denotes the occupancy at a pressure $p_{\mathrm{m}} = 0$. Upon substituting (2.7) into (2.4), we immediately recognise μ_{m}^{0} as the chemical potential of the Li atoms in an electrode subject to $p_{\mathrm{m}} = 0$ and in equilibrium with a vacancy reservoir.

Chemical potential of Li^{+} ions within the Li metal electrode

The chemical potential of the Li^{+} ions in the electroneutral metal electrode is defined in terms of the number of moles $N_{\mathrm{Li}^{+}}^{\mathrm{m}}$ of Li^{+} as

$$\mu_{\mathrm{Li}^{+}}^{\mathrm{m}} \equiv \left.\frac{\partial \mathcal{G}_{\mathrm{m}}}{\partial N_{\mathrm{Li}^{+}}^{\mathrm{m}}}\right|_{N_{\mathrm{L}}^{\mathrm{m}}}, \tag{2.8}$$

and sometimes referred to as the electrochemical potential although here we shall simply call this the chemical potential of Li^{+}. To calculate $\mu_{\mathrm{Li}^{+}}^{\mathrm{m}}$, recall that the addition of a neutral Li atom is equivalent to addition of an Li^{+} ion and an electron such that

$$\mu_{\mathrm{Li}}^{\mathrm{m}} \equiv \left.\frac{\partial \mathcal{G}_{\mathrm{m}}}{\partial N_{\mathrm{Li}}^{\mathrm{m}}}\right|_{N_{\mathrm{L}}^{\mathrm{m}}} = \left(\frac{\partial \mathcal{G}_{\mathrm{m}}}{\partial N_{\mathrm{Li^+}}^{\mathrm{m}}}\right)\left.\left(\frac{\partial N_{\mathrm{Li^+}}^{\mathrm{m}}}{\partial N_{\mathrm{Li}}^{\mathrm{m}}}\right)\right|_{N_{\mathrm{L}}^{\mathrm{m}}} + \left(\frac{\partial \mathcal{G}_{\mathrm{m}}}{\partial N_{\mathrm{el^-}}^{\mathrm{m}}}\right)\left.\left(\frac{\partial N_{\mathrm{el^-}}^{\mathrm{m}}}{\partial N_{\mathrm{Li}}^{\mathrm{m}}}\right)\right|_{N_{\mathrm{L}}^{\mathrm{m}}}, \tag{2.9}$$

where $N_{\mathrm{el^-}}^{\mathrm{m}}$ denotes the moles of electrons. Since the electrode remains electroneutral, we conduct the differentiation subject to the constraint $N_{\mathrm{Li^+}}^{\mathrm{m}} = N_{\mathrm{Li}}^{\mathrm{m}} = N_{\mathrm{el^-}}^{\mathrm{m}}$. With the chemical potential of the electrons (often referred to as the Fermi level) defined as $\mu_{\mathrm{el^-}}^{\mathrm{m}} \equiv \partial \mathcal{G}_{\mathrm{m}} / \partial N_{\mathrm{el^-}}^{\mathrm{m}}$, we have

$$\mu_{\mathrm{Li^+}}^{\mathrm{m}} = \mu_{\mathrm{Li}}^{\mathrm{m}} - \mu_{\mathrm{el^-}}^{\mathrm{m}} . \tag{2.10}$$

It is reasonable to assume that the Fermi level $\mu_{\mathrm{el^-}}^{\mathrm{m}}$ of the electrode is independent of θ_{m} and p_{m} and depends only on the electrical potential ϕ_{m} of the Li metal. Therefore, we set $\mu_{\mathrm{el^-}}^{\mathrm{m}} = -F\phi_{\mathrm{m}}$, where F is the Faraday constant and the chemical potential of the $\mathrm{Li^+}$ follows as

$$\mu_{\mathrm{Li^+}}^{\mathrm{m}} = (\mu_{\mathrm{m}}^{0} - h_{\mathrm{v}}) + F\phi_{\mathrm{m}} + p_{\mathrm{m}}(\Omega_{\mathrm{Li}} - \Omega_{\mathrm{v}}) + RT\ln\left(\frac{\theta_{\mathrm{m}}}{1-\theta_{\mathrm{m}}}\right). \tag{2.11}$$

We emphasize that (2.11) only holds for an electrode that is maintained to be electrically neutral.

Chemical potential of Li^+ ions within electrolyte

Now consider the chemical potential $\mu_{\mathrm{Li^+}}^{\mathrm{e}}$ of the $\mathrm{Li^+}$ ions within the electrolyte. Analogous to (2.11), we write $\mu_{\mathrm{Li^+}}^{\mathrm{e}}$ in terms of the Gibbs free-energy $\mathcal{G}_{\mathrm{e}}$ of the electrolyte and the number of moles $N_{\mathrm{Li^+}}^{\mathrm{e}}$ of $\mathrm{Li^+}$ ions within the electrolyte as

$$\mu_{\mathrm{Li^+}}^{\mathrm{e}} \equiv \frac{\partial \mathcal{G}_{\mathrm{e}}}{\partial N_{\mathrm{Li^+}}^{\mathrm{e}}} = \mu_{\mathrm{e}}^{0} + F\phi_{\mathrm{e}} + RT\ln\left(\frac{\theta_{\mathrm{e}}^{0}}{1-\theta_{\mathrm{e}}^{0}}\right), \tag{2.12}$$

where μ_{e}^{0} is the reference molar enthalpy of the $\mathrm{Li^+}$ ions in the electrolyte, ϕ_{e} is the electric potential of the electrolyte and there is no contribution from pressure since we have assumed $\Omega_{\mathrm{e}} = 0$. In (2.12), $\theta_{\mathrm{e}}^{0} \equiv N_{\mathrm{Li^+}}^{\mathrm{e}} / N_{\mathrm{L}}^{\mathrm{e}}$ is the occupancy of $\mathrm{Li^+}$sites within the electrolyte with $N_{\mathrm{L}}^{\mathrm{e}}$ the moles of $\mathrm{Li^+}$ sites in the electrolyte. However, since we have assumed that the electrolyte

remains electroneutral (i.e. every Li^+ cation is paired with an immobile anion within the single-ion conductor electrolyte) this occupancy is a constant.

Open circuit potential and Butler-Volmer kinetics between electrolyte/electrode

The reference quantities μ_e^0 and μ_m^0 are directly related to the open circuit (or equilibrium) potential $\mathcal{U}$ which is defined as the electrical potential that equalises the chemical potentials of Li^+ in the electrode and electrolyte in the absence of an external applied pressure and electric potential, i.e.

$$\mu_m^0 + F\mathcal{U} = \mu_e^0 + RT\ln\left(\frac{\theta_e^0}{1-\theta_e^0}\right). \tag{2.13}$$

Chemical potential definitions (2.11) and (2.12) are used in the supplementary material to derive a Butler-Volmer [22] type kinetics between the electrolyte and Li electrode (including the effect of mechanical pressure). The key assumption is that the Li concentration in the electrode is maintained in equilibrium with a vacancy reservoir and the electrical potential difference between the electrode and electrolyte keeps the Li^+ in the electrode out of the equilibrium with the Li^+ in the electrolyte. As a consequence, a flux of Li^+ between the electrolyte and electrode ensues and can be maintained. The areal current density j of Li^+ flux between the electrode and electrolyte (positive from electrode to electrolyte) is given by a Butler-Volmer type kinetics as

$$j = j_0\left\{\exp\left[\frac{(1-\beta)F\eta + p_m\Omega_v}{RT}\right] - \exp\left[\frac{-\beta F\eta - p_m(\Omega_{Li}-\Omega_v)}{RT}\right]\right\}, \tag{2.14}$$

where $\eta \equiv (\phi_m - \phi_e) - \mathcal{U}$ is the overpotential and the Butler-Volmer symmetry factor β satisfies $0 \le \beta \le 1$. The exchange current density j_0 is a function of the pressure p_m in the electrode and is related to the value $\bar{j}_0$ in the absence of an electrode pressure by

$$j_0 = \bar{J}_0 \left[\theta_{\mathrm{m}}^0 \exp\left(\frac{p_{\mathrm{m}}\Omega_{\mathrm{v}}}{RT}\right) + (1-\theta_{\mathrm{m}}^0)\right]^{-1} \exp\left[\frac{(1-\beta)p_{\mathrm{m}}(\Omega_{\mathrm{Li}}-\Omega_{\mathrm{v}})}{RT}\right]. \tag{2.15}$$

Typically, measurements are made at zero pressure so that $\bar{J}_0$ is the measured value. In (2.15), θ_{m}^0 is related to h_{v} via (2.7); readers are referred to the supplementary material for the general case in (A6) and (A7) when the metal Li is not maintained in equilibrium with a vacancy reservoir.

Chemical potential of Li^+ ions within the dendrite

The Li metal within the dendrite is assumed to be chemically identical to that in the electrode. However, while Li within the dendrite is electrically connected to the cathode, it is sandwiched within the ceramic electrolyte; consequently, vacancies cannot be generated/annihilated within the dendrite and they also cannot diffuse along the dendrite from the cathode over the timescales under consideration here. Thus, unlike the electrodes, the dendrite is not in equilibrium with a vacancy reservoir but rather the Li^+ in the dendrite is in equilibrium with the Li^+ in the electrolyte on the dendrite flanks due to the rapid exchange of Li^+ between the electrolyte and dendrite. To understand this equilibrium, we consider a case where the anode voltage Φ_{P} (without loss of generality cathode is taken to be ground) is sufficiently low that the dendrite is stationary, i.e. no flux of Li^+ across dendrite flanks and no dendrite growth resulting from flux at the dendrite tip. The general Butler-Volmer analysis, where the electrode is not in equilibrium with a vacancy reservoir (supplementary material), then dictates the value of the occupancy $\theta_{\mathrm{m}}(\xi)$ of Li sites within the dendrite to ensure no net flux across the dendrite flanks. Equivalently, this occupancy is obtained by equating the chemical potentials of the Li^+ within the dendrite and electrolyte, such that

$$\frac{1}{\theta_{\mathrm{m}}(\xi)} = 1 + \exp\left[\frac{F\eta(\xi) + p(\xi)(\Omega_{\mathrm{Li}}-\Omega_{\mathrm{v}}) - h_{\mathrm{v}}}{RT}\right]. \tag{2.16}$$

Here, ξ is an intrinsic co-ordinate measured along the dendrite length (Fig. 1a), $\eta(\xi) \equiv -(\phi_{\mathrm{d}}(\xi) + \mathcal{U})$ is the overpotential at location ξ in terms of the electric potential ϕ_{d} in the electrolyte. The pressure $p(\xi)$ is assumed to be equal to that in the electrolyte along the dendrite flanks (consistent with the small strain elastic dislocation stress field of the dendrite discussed in Section 2.2.5 and detailed in the supplementary material). Upon recalling that $h_{\mathrm{v}} \approx 50\ \mathrm{kJ\ mol^{-1}}$ [21], we recognise that $\theta_{\mathrm{m}} \approx 1$ and only a very small flux of $\mathrm{Li^{+}}$ is required across the dendrite flanks to ensure that this equilibrium condition is maintained even if $\eta(\xi)$ and $p(\xi)$ were to change with dendrite growth. We recognise from (2.16) that the chemical potential of Li within the dendrite varies along ξ and there is a tendency for this chemical potential to equalise via diffusion of vacancies along the length of the dendrite. However, this diffusion is negligible over the timescales of interest.

2.2 Electrochemical/mechanical constitutive and balance laws

The governing constitutive and balance laws for the electric and stress fields are now recapitulated; see for example [23] for a more extensive discussion on the balance laws. Our aim is to model dendrite growth in the electrolyte and hence we treat the electrodes as equipotential surfaces of vanishing volume which removes the need to specify constitutive laws for the electrodes. The electrolyte is modelled as an isotropic linear elastic solid allowing for the flux of $\mathrm{Li^{+}}$ in addition to an isotropic linear dielectric response. For the sake of brevity of notation, we omit the usual subscript "e" for "electrolyte" such that $\phi_{\mathrm{e}} \to \phi$ in the following discussion; Cartesian tensor notation is employed.

2.2.1 Electrical constitutive model and balance laws

First, consider the electrolyte. Gauss's law for a linear dielectric of permittivity $\mathcal{E}$ requires that the electric field E_i satisfies $\mathcal{E}E_{i,i} = \rho_{\mathrm{f}}$ where ρ_{f} is the density of free-charge. Further, in

electrostatics the Maxwell-Faraday equation (Faraday's law of induction) is automatically satisfied by defining $E_i \equiv -\phi_{,i}$ and thus Gauss's law reduces to $\mathcal{E}\phi_{,ii} = -\rho_{\mathrm{f}}$. We restrict our analysis to an electroneutral electrolyte where the occupancy of the Li^+ remains fixed at θ_{e}^0; consequently $\rho_{\mathrm{f}} \equiv 0$ and Gauss's law for the electrolyte and the surrounding free-space reduces to

$$\phi_{,ii} = 0. \tag{2.17}$$

This is the basic governing electrical balance law that needs to be solved with relevant boundary conditions which are discussed in Section 2.2.4.

2.2.2 Mechanical constitutive relationship and balance laws

The electrolyte is taken to be a linear elastic solid with a shear modulus G and Poisson's ratio ν. Assume that small strain conditions prevail and, in the global co-ordinate system x_i, define strain from the displacement field u_i as $\varepsilon_{ij} \equiv (u_{i,j} + u_{j,i})/2$ with the material stress σ_{ij} related to ε_{ij} via Hooke's law,

$$\varepsilon_{ij} = \frac{\sigma_{ij}}{2G} - \frac{\nu}{2G(1+\nu)}\sigma_{kk}\delta_{ij}, \tag{2.18}$$

where δ_{ij} is the usual Kronecker delta. The Lorentz forces on the free-charges within the electrolyte generate body forces that are typically written in terms of the Maxwell stresses

$$\sigma_{ij}^{\mathrm{M}} = \mathcal{E}\left(E_i E_j - \frac{1}{2}E_k E_k \delta_{ij}\right), \tag{2.19}$$

such that the body forces are $-\sigma_{ij,j}^{\mathrm{M}}$. In the presence of these body forces associated with the electric field E_i, the mechanical equilibrium, equation reads

$$\sigma_{ij,j} + \sigma_{ij,j}^{\mathrm{M}} = 0 \tag{2.20}$$

Recall that for an electroneutral electrolyte that is also assumed to be a linear dielectric, $E_{i,i} = 0$. It therefore follows that $\sigma_{ij,j}^{\mathrm{M}} = 0$ and the mechanical balance law reduces to $\sigma_{ij,j} = 0$ with

the Maxwell stresses only affecting the traction boundary conditions as will be discussed in Section 2.2.4.

2.2.3 Flux of Li in the electrolyte

Gradients of the chemical potential of Li^+ within the electrolyte provide the driving force $f_i \equiv -\partial \mu^{\mathrm{e}}_{\mathrm{Li}^+}/\partial x_i$ for the flux of Li^+. The molar flux in the electroneutral electrolyte is $h_i \equiv mN^{\mathrm{e}}_{\mathrm{L}}\theta^0_{\mathrm{e}} f_i$, where m is the mobility of Li^+ in the electrolyte. Typically, this flux is measured in terms of the current density $j_i = Fh_i$ of the Li^+ ions, with the mobility written in terms of an ionic conductivity defined as $\kappa \equiv j_1/E_1$ for an electrical field applied in the $1-$direction. Thus, setting $\kappa = mN^{\mathrm{e}}_{\mathrm{L}}\theta^0_{\mathrm{e}}F$, the current is related to the gradient of the electric potential as $j_i = -\kappa\phi_{,i}$ which is essentially a statement of Ohm's law (there is no diffusive contribution to the flux as the electrolyte is assumed to remain electroneutral with the occupancy of Li^+ sites fixed at θ^0_{e}). Conservation of Li^+ ions requires

$$FN^{\mathrm{e}}_{\mathrm{L}}\dot{\theta}_{\mathrm{e}} = -j_{i,i}. \tag{2.21}$$

However, since we are constraining the electrolyte to remain electroneutral this implies that $\dot{\theta}_{\mathrm{e}} = 0$ and the flux balance law reduces to $\phi_{,ii} = 0$, i.e. identical to Eq. (2.17). Thus, for the electroneutral electrolyte with $\Omega_{\mathrm{e}} = 0$, the electrical and Li^+ flux balance laws reduce to a single governing equation given by the Laplace equation $\phi_{,ii} = 0$ that needs to be solved with appropriate boundary conditions. We emphasize that this reduction in number of the independent governing equations implies that no solutions exist for certain problems (e.g. electrolyte loaded by blocking electrodes that impose an electrical potential across the electrolyte but prohibit the flux of Li^+ across the electrolyte/electrode interfaces). However, the electroneutrality assumption admits solutions for the boundary value problems analysed here and hence this simplification is considered appropriate for this study.

2.2.4 Boundary conditions

We shall discuss boundary conditions for the mechanical and electrical/flux balance laws along three interfaces: (i) the electrode/electrolyte interfaces; (ii) the flanks of a dendrite corresponding to the electrolyte/dendrite interface and (iii) the electrolyte/free-space interface (Fig. 2). We restrict our analysis to a two-dimensional (2D) plane strain situation with deformation constrained to the $(x_1 - x_2)$ plane and an electrolyte of thickness B in the x_3 −direction.

First, consider the mechanical balance laws with boundary conditions on the external boundaries of the electrolyte and along the dendrite flanks. The external surfaces $\mathcal{S}$ of the electrolyte are subjected to tractions T_i^0 and will generate stresses within the electrolyte. A dendrite is associated with a normal displacement jump $\Delta u_{\mathrm{n}} = b$ across corresponding material points P and Q on opposite flanks of the dendrite, i.e. Δu_{n} is defined in terms of the displacements u_i^{P} and u_i^{Q} of material points P and Q as $\Delta u_{\mathrm{n}} \equiv \left(u_i^{\mathrm{P}} n_i^{\mathrm{P}} + u_i^{\mathrm{Q}} n_i^{\mathrm{Q}}\right)$ where n_i^{P} and n_i^{Q} are the outward normals to the electrolyte at material points P and Q, respectively, along the dendrite flanks (Fig. 2). The mechanical equilibrium equation (2.19) is then solved with these two sets of boundary conditions. However, it is worth emphasizing that Maxwell stresses σ_{ij}^{M} along $\mathcal{S}$ in the electrolyte[i] need to be considered while applying the boundary conditions on $\mathcal{S}$. As shown in Fig. 2, with T_i^0 the applied external tractions due to purely mechanical loading, the boundary conditions on $\mathcal{S}$ are $T_i \equiv \sigma_{ij} n_j = T_i^0 - \sigma_{ij}^{\mathrm{M}} n_j$, where n_j is the unit outward normal to the electrolyte.

[i] We do not need to consider the Maxwell stresses in the electrodes or free-space along the electrolyte/electrode and electrolyte/free-space interfaces. The Maxwell stresses in the electrodes vanish as the electric field is zero, and the normal component of the electric field in free-space also vanishes due to the zero-flux boundary condition along those interfaces (see supplementary material for a more detailed discussion). Thus, the Maxwell stresses in free-space do not contribute to the traction boundary condition on the electrolyte.

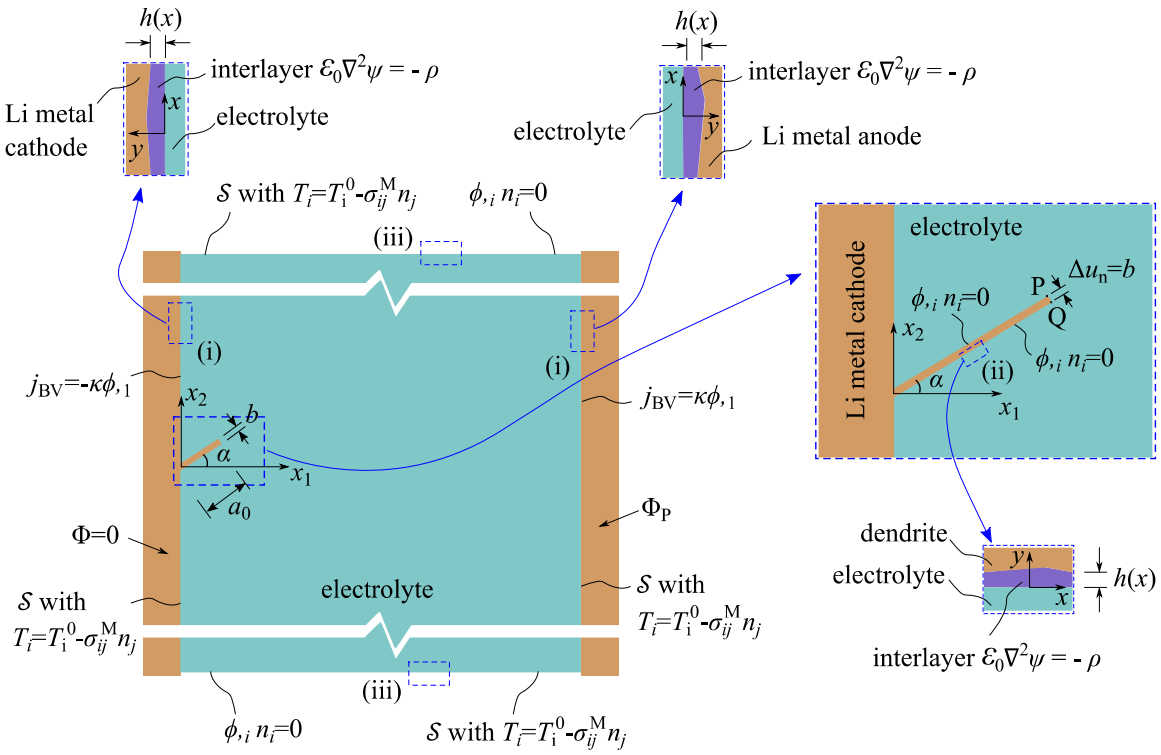

Figure 2: A sketch showing the electrochemical and mechanical boundary conditions imposed on the electrolyte with j_{BV} denoting the Butler-Volmer flux specified in (2.14). The three types of interfaces, (i)-(ii)-(iii), are indicated while the insets show an interlayer of thickness $h(x)$ that is formed between the electrolyte and Li electrodes and along the flanks of the dendrite to ensure that $\mathrm{curl}(E_i) = 0$; see supplementary material for a detailed discussion.

Boundary conditions for the electrical/flux balance laws (2.17) need to be considered along the electrolyte/electrode interfaces as well as along the dendrite flanks and interfaces with free-space. We impose Butler-Volmer conditions along the electrode/electrolyte interfaces; e.g. for the symmetric cell in Fig. 2 loaded by an anode maintained at an electrical potential Φ_{P}, this condition along the anodic interface located at $x_1 = L$ is

$$\left.\frac{\partial \phi}{\partial x_1}\right|_{x_1=L} = \frac{j_0}{\kappa}\left\{\exp\left[\frac{(1-\beta)F(\Phi_{\mathrm{P}}-\phi_{\mathrm{A}}-\mathcal{U})+p_{\mathrm{m}}\Omega_{\mathrm{v}}}{RT}\right]\right. \\ \left. -\exp\left[\frac{-\beta F(\Phi_{\mathrm{P}}-\phi_{\mathrm{A}}-\mathcal{U})-p_{\mathrm{m}}(\Omega_{\mathrm{m}}-\Omega_{\mathrm{v}})}{RT}\right]\right\}, \tag{2.22}$$

where $\phi_{\mathrm{A}}(x_2) = \phi(x_1 = L, x_2)$ is the potential in the electrolyte at the electrolyte/anode interface. A similar condition can also be written for the cathode/electrolyte interface. Following the discussion in Section 2.1, we require that the flux of Li^+ across the dendrite flanks to vanish. Equally, the flux across the interfaces with free-space also vanishes (as Li^+ fluxing out of the electrolyte there cannot acquire an electron). Thus, along all these interfaces we impose the Neumann boundary conditions $\phi_{,i} n_i = 0$ where n_i is the normal to the respective electrolyte surfaces. These boundary conditions are sufficient to solve the Laplace equation (2.17) but require some clarifications with regard to their implications for Gauss's law and the Maxwell-Faraday equation along the interfaces; see supplementary material for a detailed discussion.

2.2.5 Analytical solution for the mechanical field of a dendrite

The mechanical balance law (2.19) is decoupled from the flux and electrical balance laws with the electric loading only appearing through the Maxwell stresses that enter as boundary tractions. The problem thus reduces to calculation of the stress/strain fields in the electrolyte containing a dendrite modelled as an edge dislocation with Burgers vector of magnitude b and subject to the traction boundary conditions on $\mathcal{S}$. The elastic field of the dislocation is singular and following [24] we write the total stress field σ_{ij} as a superposition of the analytically-known singular field $\tilde{\sigma}_{ij}$ of an edge dislocation in an infinite medium and a non-singular field $\hat{\sigma}_{ij}$ that corrects for the boundary conditions, i.e. $\sigma_{ij} = \tilde{\sigma}_{ij} + \hat{\sigma}_{ij}$. Since $\tilde{\sigma}_{ij,j} = 0$, we require that the so-called image field $\hat{\sigma}_{ij}$ is also divergence-free to ensure that (2.19) is satisfied. This

non-singular image field can therefore be calculated in the general case by a finite element (FE) analysis but also analytically in some cases.

There are two quantities from these mechanical fields of specific interest in Section 2.3 to evaluate the conditions for dendrite growth and here we focus on these: (i) the pressure field immediately ahead of the dendrite and (ii) the change in mechanical potential energy of the entire system (battery) due to propagation of the of the dendrite. In the supplementary material, we demonstrate that the dendrite tip pressure is purely due to the image stresses, i.e. $\hat{p}_{\text{tip}} \equiv -\hat{\sigma}_{kk}^{\text{tip}}/3$, where $\hat{\sigma}_{ij}^{\text{tip}}$ are the components of $\hat{\sigma}_{ij}(x_i)$ at the dendrite tip with the singular $\tilde{\sigma}_{ij}$ field not contributing to the dendrite tip pressure. The change in the mechanical potential energy $\Delta\Pi$ of the entire system (battery) due to propagation of the of the dendrite of length a_0 by a distance Δa (Fig. 1a) is typically written, in terms of dislocation analyses, as $\Delta\Pi \equiv f_{\text{climb}}(B\Delta a)$, where f_{climb} is the climb component of the Peach-Koehler force. Here, we have used the fact that the dendrite length increases along the positive $\xi-$direction and standard dislocation analysis [25] then specifies $f_{\text{climb}} = -\hat{\sigma}_{ij}^{\text{tip}} b m_i m_j$ where m_i is a unit vector perpendicular to the dendrite (Fig. 1a) and $\hat{\sigma}_{ij}^{\text{tip}}$ the value of $\hat{\sigma}_{ij}$ at the dendrite tip. This image field is non-singular and of primary interest at the dendrite tip.

For an electrolyte of arbitrary geometry, f_{climb} is determined by numerically calculating $\hat{\sigma}_{ij}$; see for example [26]. However, analytical solutions serve as excellent approximations for many typical battery geometries. In particular, consider the case where the length a_0 of the dendrite at the point of initiation of growth is much less than all leading dimensions of the electrolyte. Therefore, it suffices to approximate the geometry as a dendrite within a half-space for which there exists an analytical solution for both $\hat{\sigma}_{ij}$ and σ_{ij}; see supplementary material. For a

dendrite of length a_0 and Burgers vector magnitude b emanating from the cathodic surface at an angle α (Fig. 1a), the climb Peach-Koehler force is

$$f_{\text{climb}} = \frac{Gb^2}{4\pi(1-\nu)a_0} - b(\Sigma_{11}\sin^2\alpha + \Sigma_{22}\cos^2\alpha)\,, \tag{2.23}$$

where Σ_{11} and Σ_{22} are remote uniform biaxial stresses applied to the electrolyte as shown in Fig. 1a. Moreover, since the dendrite tip pressure is solely due to the image stresses, $\hat{p}_{\text{tip}} = -(\Sigma_{11}+\Sigma_{22})(1+\nu)/3$.

A unique feature of modelling the dendrites as dislocations is that, in the absence of external applied tractions, the stress σ_{ij} vanishes at the root of the dendrite and thus the Li within the dendrite exerts no pressure on the Li cathode. Most previous studies have analysed dendrites as internally pressurised cracks [17-19] with a pressure p_{Li}. However, since dendrites open into the cathode such cracks exert an indentation pressure p_{Li} on the cathode. The metallic cathode cannot sustain an indentation pressure greater than the deep penetration pressure which is on the order of $5Y$ [27] where Y is the yield strength of the cathode material. Setting $Y \approx 5$ MPa as the yield strength of Li, this restricts the crack pressure to less than 25 MPa. Typically, an internal pressure of approximately 1 GPa is required to initiate crack growth in ceramic electrolytes [19] and therefore the growth of dendrites in such a pressurised crack mode is precluded as already recognised in [17]. The dislocation mode proposed here does not have this issue as the Li within the dislocation-like dendrite exerts no pressure on the cathode.

2.3 Mechanism of dendrite propagation via fracture at constant chemical potential

The constitutive equations and balance laws detailed above can be used to calculate the electric potential and stress fields at the tip of the stationary dendrite and we now use these to understand the conditions under which the propagation of the dendrite can initiate. Consider a

dendrite as shown in Fig. 1a and recall that the Li occupancy of Li sites within the dendrite is such that the chemical potential of the Li^+ within the dendrite is equal to that of the Li^+ in the adjacent electrolyte along the length ξ of the dendrite and this includes the dendrite tip. Thus, propagation of the dendrite, if it occurs, takes place with no jump in chemical potential μ_{tip} of the Li^+ at the dendrite tip. The propagation of the dendrite by a distance Δa involves (i) fracture of the electrolyte at the dendrite tip; (ii) creation of the volume $Bb\Delta a$ at the dendrite tip by elastic deformation of the electrolyte and (iii) fluxing of Li^+ from electrolyte into the dendrite at constant chemical potential to fill this empty space, with the Li^+ in the dendrite acquiring electrons from the cathode so as to maintain electrical neutrality. We consider this to be an equilibrium process (at constant temperature and chemical potential μ_{tip} of Li^+) and are interested in the free-energy change associated with this process.

To evaluate the free-energy change associated with dendrite propagation, we consider a spatially uniform system that is representative of a material point in the electrolyte directly ahead of the dendrite tip (the inset in Fig. 1a). The system is of arbitrary dimensions and without loss of generality we shall set the system to be a cuboid of dimension $\Delta a \times \hbar \times B$, where $\hbar$ is a length measured perpendicular to the dendrite, B is the thickness of the system in the x_3 −direction and equal to the thickness of the electrolyte; the length of the system in the direction along the dendrite is set equal to the length Δa by which we assume the dendrite propagates (Fig. 1a). The system is in equilibrium with a reservoir maintained at a constant chemical potential μ_{tip} of Li^+ and temperature T (Fig. 1b). With ϕ_{tip} denoting the electric potential at the dendrite tip this chemical potential is given by (2.12) as

$$\mu_{\text{tip}} = \mu_{\text{e}}^0 + F\phi_{\text{tip}} + RT\ln\left(\frac{\theta_{\text{e}}^0}{1-\theta_{\text{e}}^0}\right). \tag{2.24}$$

It now remains to specify the other independent (natural) variables of the system. The mechanical field of the dislocation comprises the singular infinite body ($\widetilde{\ }$) field that is invariant at the dendrite tip with respect to the location of the tip and the finite image ($\widehat{\ }$) fields. Since we are only concerned with change in the state of the system due to dendrite propagation, we only consider the stress $\hat{\sigma}_{ij}^{\mathrm{tip}}$ and conjugated strain $\hat{\varepsilon}_{ij}^{\mathrm{tip}}$. It is however convenient to define stress and strain components $\hat{\sigma}_{ij}^{\prime\,\mathrm{tip}}$ and $\hat{\varepsilon}_{22}^{\prime\,\mathrm{tip}}$ in a co-ordinate system x_i' rotated α with respect to x_i (see Fig. 1a). To allow for fracture of the electrolyte, we shall consider a mixed situation where all components of $\hat{\varepsilon}_{22}^{\prime\,\mathrm{tip}}$ of the system are held fixed except $\hat{\varepsilon}_{22}^{\prime\,\mathrm{tip}}$ so as to allow the system to expand and allow the dendrite to propagate in the positive $x_1' -$ direction. Rather, instead of a fixed $\hat{\varepsilon}_{22}^{\prime\,\mathrm{tip}}$ we impose a fixed stress $\hat{\mathcal{T}} = \hat{\sigma}_{ij}^{\mathrm{tip}} m_i m_j$. Then the change in potential energy of the entire system (battery) is $\Delta\Pi = -(\hat{\mathcal{T}} B \Delta a) b$ with $\hat{\mathcal{T}} \equiv -f_{\mathrm{climb}}/b$.

Now consider the fractured state of the electrolyte, as shown in Fig. 1c, where a metal phase of thickness b is sandwiched between and adhered to the fractured electrolyte. This metal phase comprises N moles of Li and since it is connected to the cathode is maintained at an electric potential $\phi_{\mathrm{m}} = 0$. On the other hand, the electrochemical and mechanical state of the two halves of the fractured electrolyte remains unaltered from that in the intact state. Upon recalling that Li^+ in the metal phase is in equilibrium with the Li^+ in the reservoir and electrolyte, the occupancy θ_{tip} of lattice sites within the metal phase at the dendrite tip is given by (2.16) as

$$\frac{1}{\theta_{\mathrm{tip}}} = 1 + \exp\left[\frac{F\eta_{\mathrm{tip}} + \hat{p}_{\mathrm{tip}}(\Omega_{\mathrm{Li}} - \Omega_{\mathrm{v}}) - h_{\mathrm{v}}}{RT}\right], \tag{2.25}$$

where $\eta_{\text{tip}} \equiv -(\phi_{\text{tip}} + \mathcal{U})$ is the overpotential of the electrolyte with respect to the metal phase. We emphasize that the dendrite tip pressure only has contributions from the image stress as discussed in Section 2.2.5 and hence remains finite.

We are now in a position to calculate the change in free-energy of the system resulting from this fracture process, i.e. calculate the difference in the free-energy between the unfractured and fractured state that we shall refer to as states B and A, respectively (Figs. 1b and 1c, respectively). The appropriate free-energy, labelled here as $\mathcal{L}_{\text{tip}}$ needs to be defined by recalling that while the stress $\hat{\mathcal{T}}$ and chemical potential μ_{tip} of the Li^+ are held constant in the fracture process (i.e. need to be natural variables of $\mathcal{L}_{\text{tip}}$), the other natural variables are those of the Helmholtz free-energy of the system. Thus, taking the appropriate Legendre transforms, the free-energy of the system in state A with N_{Li^+} moles of Li^+ is given in terms of the Helmholtz free-energy $A_{\text{tip}}^{(\text{A})}$ as

$$\mathcal{L}_{\text{tip}}^{(\text{A})} = A_{\text{tip}}^{(\text{A})} - \left(\hat{\mathcal{T}} B \Delta a\right)\left(\hat{\varepsilon}_{22}'^{\,\text{tip}} \hbar\right) - \mu_{\text{tip}} N_{\text{Li}^+}\,, \tag{2.26}$$

where

$$\hat{\mathcal{T}} \equiv \frac{1}{(B\hbar\Delta a)} \frac{\partial A_{\text{tip}}^{(\text{A})}}{\partial \hat{\varepsilon}_{22}'^{\,\text{tip}}} \quad \text{and} \quad \mu_{\text{tip}} \equiv \frac{\partial A_{\text{tip}}^{(\text{A})}}{\partial N_{\text{Li}^+}}. \tag{2.27}$$

In (2.27), the partial derivatives are taken with all other natural variables of $A_{\text{tip}}^{(\text{A})}$ held fixed.

In state B, the two halves of the fractured electrolyte are in the same state as in state A and the only differences between the two states are that state B has (i) two new electrolyte/Li metal interfaces each with an energy $\gamma_{\text{e/Li}}$ per unit area[ii]; (ii) an electroneutral metal phase comprising

[ii] In terms of the surface energy γ_{e} of electrolyte, the surface energy γ_{Li} of Li and the work of adhesion W_{adh} between electrolyte and Li, the energy of the electrolyte/Li interface is given by the Born-Haber cycle as $\gamma_{\text{e/Li}} = \gamma_{\text{e}} + \gamma_{\text{Li}} - W_{\text{adh}}$.

N moles of Li^+ and N moles of electrons and (iii) the system has strained by a nominal strain $b/\hbar$ in the x_2' −direction with respect to state A. Then, analogous to (2.26) the free-energy of state B is

$$\mathcal{L}_{\mathrm{tip}}^{(\mathrm{B})} = \left(A_{\mathrm{tip}}^{(\mathrm{A})} + A_{\mathrm{m}}\right) + 2\gamma_{\mathrm{e/Li}} B\Delta a - \left(\hat{\mathcal{T}} B\delta a\right)\left(\hat{\varepsilon}_{22}'^{\,\mathrm{tip}}\hbar + b\right) - \mu_{\mathrm{tip}}\left(N_{\mathrm{Li}^+} + N\right), \qquad (2.28)$$

where A_{m} is the Helmholtz free-energy of the metal phase. This metal phase comprises Li atoms much like the electrodes but with a different occupancy of Li sites. Thus, it suffices to use the analysis of Section 2.1 to evaluate A_{m}. Using the fact that $\phi_{\mathrm{m}} = 0$ and that the total number of lattice sites in the metal phase is $N_{\mathrm{L}}^{\mathrm{m}} = N/\theta_{\mathrm{tip}}$ with θ_{tip} given by (2.25), A_{m} follows from (2.3) as

$$A_{\mathrm{m}} = N\mu_{\mathrm{m}}^0 + N\left(\frac{1}{\theta_{\mathrm{tip}}} - 1\right)h_{\mathrm{v}} - \left(\frac{N}{\theta_{\mathrm{tip}}}\right)Ts_{\mathrm{tip}}, \qquad (2.29)$$

where the specific entropy is

$$s_{\mathrm{tip}} \equiv -R\left[\theta_{\mathrm{tip}}\ln\theta_{\mathrm{tip}} + \left(1-\theta_{\mathrm{tip}}\right)\ln\left(1-\theta_{\mathrm{tip}}\right)\right]. \qquad (2.30)$$

Then, the change in free-energy of system upon fracture is

$$\Delta\mathcal{L}_{\mathrm{tip}} \equiv \mathcal{L}_{\mathrm{tip}}^{(\mathrm{B})} - \mathcal{L}_{\mathrm{tip}}^{(\mathrm{A})} = 2\gamma_{\mathrm{e/Li}} B\Delta a + A_{\mathrm{m}} - \left(\hat{\mathcal{T}} B\Delta a\right)b - \mu_{\mathrm{tip}}N. \qquad (2.31)$$

Using $N = \rho_{\mathrm{m}} bB\Delta a$, where $\rho_{\mathrm{m}} = 1/\Omega_{\mathrm{Li}}$ is the theoretical molar density of Li and μ_{tip} is given by (2.24), we obtain

$$\frac{\Delta\mathcal{L}_{\mathrm{tip}}}{B\Delta a} = 2\gamma_{\mathrm{e/Li}} + \rho_{\mathrm{m}} b\left[F\eta_{\mathrm{tip}} - Ts_{\mathrm{tip}} + \left(\frac{1}{\theta_{\mathrm{tip}}} - 1\right)h_{\mathrm{v}}\right] - b\hat{\mathcal{T}}, \qquad (2.32)$$

where we have used the definition (2.13) of the $\mathcal{U}$ along with $\eta_{\mathrm{tip}} \equiv -(\phi_{\mathrm{tip}} + \mathcal{U})$. Now recognise that the process of transforming the system from state A to B is spontaneous if $\Delta\mathcal{L}_{\mathrm{tip}} \leq 0$ (with $\Delta a > 0$), implying that the condition for dendrite growth is

$$2\gamma_{\mathrm{e/Li}} + \rho_{\mathrm{m}} b\left[F\eta_{\mathrm{tip}} - Ts_{\mathrm{tip}} + \left(\frac{1}{\theta_{\mathrm{tip}}} - 1\right)h_{\mathrm{v}}\right] - b\hat{\mathcal{T}} \leq 0. \qquad (2.33)$$

We label the critical dendrite tip overpotential required to initiate dendrite growth as η_{c} and using the equality in (2.33), this critical overpotential is

$$\eta_{\mathrm{c}} = \frac{b\hat{\mathcal{T}} - 2\gamma_{\mathrm{e/Li}}}{F\rho_{\mathrm{m}}b} + \frac{1}{F}\left[Ts_{\mathrm{tip}} - \left(\frac{1}{\theta_{\mathrm{tip}}} - 1\right)h_{\mathrm{v}}\right]. \tag{2.34}$$

This analysis provides the conditions to be met at the dendrite tip to initiate dendrite growth. With $\hat{\mathcal{T}}b = -f_{\mathrm{climb}}$ known, the critical dendrite-tip overpotential (2.34) can explicitly be written as

$$\eta_{\mathrm{c}} = \frac{1}{F}\left[Ts_{\mathrm{tip}} - \left(\frac{1}{\theta_{\mathrm{tip}}} - 1\right)h_{\mathrm{v}}\right] - \frac{2\gamma_{\mathrm{e/Li}} + f_{\mathrm{climb}}}{F\rho_{\mathrm{m}}b}. \tag{2.35}$$

It is worth emphasising that for $h_{\mathrm{v}}/(RT) \gg 1$, $\theta_{\mathrm{tip}} \to 1$ and $s_{\mathrm{tip}} \to 0$ and (2.35) simplifies to

$$\eta_{\mathrm{c}} \approx -\frac{2\gamma_{\mathrm{e/Li}} + f_{\mathrm{climb}}}{F\rho_{\mathrm{m}}b}, \tag{2.36}$$

and this expression suffices to a very high degree of accuracy for the room temperature behaviour of the Li-based systems considered here.

3. Prediction of the initiation of dendrite growth

In order to illustrate the key phenomena in a simple manner, we restrict the bulk of our predictions to an initial dendrite of length a_0 emanating at right angles from the cathodic interface ($\alpha = 0^{\mathrm{o}}$), with zero external tractions applied to the electrolyte (i.e. we are also neglecting the tractions generated by the negligible Maxwell stresses[iii]). Moreover, we assume that the electrodes completely cover the electrolyte surfaces along $x_1 = 0$ and $x_1 = L$ (Fig. 1a). Some additional simulations on the effect of the dendrite orientation and effect of external applied mechanical loads are discussed in the Supplementary material. The electrolyte is taken

[iii] Typical electric fields rarely exceed 1000 Vm^{-1} (1 V applied over an electrolyte of thickness 1 mm). Given that the relative permittivity of LLZO ≈ 50 [28], the Maxwell stresses associated with this electric field are on the order of 10^{-4} Pa and are hence negligible compared to the stresses generated by the dendrite which can be in the GPa range near the dendrite tip.

to be LLZO for which all required parameters have either been directly experimentally measured or computed from density functional theory (DFT) calculations. Table 2 summarizes the majority of material parameters for Li/LLZO/Li symmetric cell. All results are presented at a temperature $T = 300$ K and for an electrolyte of thickness $L = 1000$ μm and width $W = 10L$, in line with a large number of experiments [8-12]. However, we emphasize that the results in terms of a critical current density to initiate dendrite growth are insensitive to L whereas the applied anodic voltages to drive these currents scale with L. Table 2 does not include the exchange current $\bar{j}_0$, the symmetry factor β and the open circuit potential $\mathcal{U}$ which remain to be specified. In the supplementary material we discuss the relation of these parameters to the interfacial resistance Z and here we report predictions over approximately the range $3\ \Omega\text{cm}^2 < Z < 500\ \Omega\text{cm}^2$ in line with values reported in the literature.

Table 2: Summary of material parameters for the Li/LLZO/Li symmetric cell. The electrode/electrolyte interfacial resistances are discussed within the text.

Material parameter	**Symbol**	**Value**	**Ref.**
Shear modulus of LLZO	G	60 GPa	[29]
Poisson's ratio of LLZO	ν	0.2	[29]
Conductivity of LLZO	κ	0.46 mS cm^{-1}	[9]
Surface energy of LLZO	γ_{LLZO}	0.84 J m^{-2}	[8]
Surface energy of Li	γ_{Li}	0.45 J m^{-2}	[8]
Work of adhesion between LLZO and Li	W_{adh}	0.67 J m^{-2}	[8]
Theoretical molar density of Li	$\rho_{\text{m}} \equiv 1/\Omega_{\text{Li}}$	76286 mol m^{-3}	standard
Enthalpy of vacancy formation in Li	h_{v}	50 kJ mol^{-1}	[21]

Predictions are presented for two cases: (i) ideal electrical contact between the cathode and electrolyte, i.e. Z is spatially uniform over the interface and (ii) the situation where a void of size ℓ forms on the interface such that all contact is lost between the electrolyte and cathode over this region. In all cases, Z is spatially uniform over the anode/electrolyte interface.

3.1 Ideal electrical contact between electrodes and electrolyte

The focus of our calculations is on determining the current densities that initiate dendrite growth and we consider the case of loading of the symmetric cell by a nominal current density j_∞ (j_∞ is positive for current in the positive x_1 −direction). For a dendrite with Burgers vector of magnitude $b \ll W$, the presence of a stationary dendrite has a negligible effect on the electric field within the electrolyte. The governing equation for the electric potential within the electrolyte reduces to a one-dimensional Laplace's equation which can be readily solved analytically with the nonlinear Butler-Volmer boundary conditions (2.14) at the electrode/electrolyte interfaces. The overpotential in the electrolyte at the dendrite tip is given by

$$\eta_{\text{tip}} = \frac{j_\infty a_0}{\kappa} + \frac{2RT}{F}\sinh^{-1}\left(\frac{j_\infty ZF}{2RT}\right) \approx j_\infty\left(Z + \frac{a_0}{\kappa}\right), \tag{3.1}$$

where the approximation assumes $j_\infty ZF/(2RT) \ll 1$. Equating η_{tip} to η_{c} as stated in (2.35) then furnishes the minimum current $-j_\infty = i_{\min}$ required to initiate dendrite growth in the electrolyte as a function of b. These predictions are presented in Fig. 3a for the choice of interfacial resistance $Z = 5\ \Omega\text{cm}^2$ and selected values of the initial dendrite length a_0. For any given a_0, $i_{\min}$ displays a minimum value with respect to b and this is best understood by developing an approximate expression for $i_{\min}$ by employing the approximation (2.36) for η_{c} and the linearized form in (3.1). The closed-form expression for $i_{\min}$ using these approximations is

$$i_{\min} \approx \frac{1}{F\rho_{\text{m}}\left(Z + \frac{a_0}{\kappa}\right)}\left[\frac{2\gamma_{\text{e/Li}}}{b} + \frac{Gb}{4\pi(1-\nu)a_0}\right], \tag{3.2}$$

and predictions of (3.2) are included in Fig. 3a as dashed lines: there is remarkable agreement with the full analysis where (2.35) is employed along with the non-linear Butler-Volmer conditions. The fact that $i_{\min}$ has a minimum with respect to b is also clearly seen from (3.2) and is understood as follows. Increasing b enhances the driving force for dendrite growth as

more Li^+ transits from the electrolyte into the dendrite resulting in a larger release of electrical energy. Conversely the higher b also increases the elastic energy required to wedge open the electrolyte and allow dendrite growth. These two opposing effects of increasing b give rise to the minimum seen in Fig. 3a.

The question remains as to what sets the critical current density i_{CCD} typically reported in experiments [8, 9]? The current i_{min} required to initiate dendrite growth is minimised for a Burgers vector of magnitude $b = b_{\mathrm{CCD}}$ and for a given value of a_0, as seen in Fig. 3a. We hypothesize that there exists a distribution of slits in the electrolyte that emanate from the surface of the electrolyte and each of these slits has a specific value of Burgers vector magnitude b associated with the atomic configuration at the slit tip. These initial slits are filled with Li during the cyclic loading of the cell and form initial dendrites characterised by a combination (a_0, b). For a given initial length a_0, the dendrite with Burgers vector magnitude b_{CCD} will grow at the lowest current and we label this value of i_{min} as i_{CCD} (Fig. 3a). Predictions of b_{CCD} versus initial dendrite length a_0 are included in Fig. 3b. This relation has negligible dependence on Z which can be immediately seen by minimising the approximate value of i_{min} in (3.2) to give

$$b_{\mathrm{CCD}} \approx \sqrt{\frac{8\pi(1-\nu)a_0\gamma_{\mathrm{e/Li}}}{G}}. \tag{3.3}$$

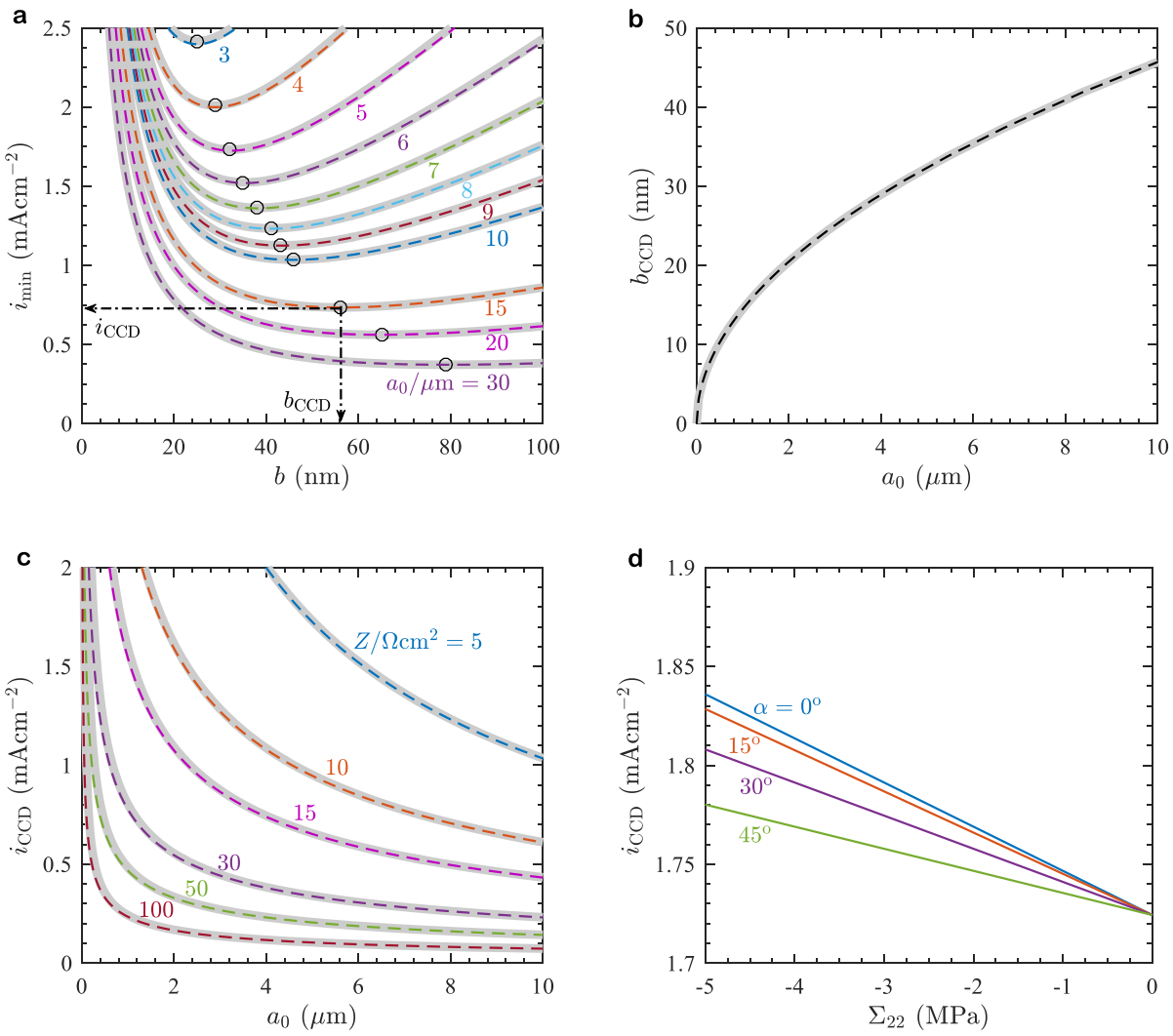

Figure 3: Predictions (thick grey solid lines: full analysis; dashed lines: approximation) of (a) the minimum cell current $i_{\rm min}$ required to initiate dendrite growth as a function of the Burgers vector b in a symmetric cell with interfacial resistance $Z = 5\,\Omega{\rm cm}^{-2}$ (b) $b_{\rm CCD}$ as a function of initial dendrite length a_0 (independent of Z) and (c) the critical current density $i_{\rm CCD} \equiv \min_b(i_{\rm min})$ as a function of the initial dendrite length for selected values of the interfacial resistance Z. (d) The effect on $i_{\rm CCD}$ of an external compressive stress Σ_{22} applied to the electrolyte. Results are shown for a dendrite of length $a_0 = 5\,\mu$m, $Z = 5\,\Omega{\rm cm}^{-2}$ and selected values of the dendrite angle α; see supplementary for a discussion of these results.

Predictions of this approximate expression are included in Fig. 3b (as dashed lines) and are nearly indistinguishable from the full calculations. The corresponding predictions of $i_{\rm CCD}$ are

included in Fig. 3c as a function of a_0 for selected values of Z. The predictions of the approximate analysis are also included (i_{CCD} calculated by substituting $b = b_{\mathrm{CCD}}$ from (3.3) into (3.2)) and again show excellent agreement with the full predictions. The predictions suggest that i_{CCD} reduces with increasing a_0 and Z. The fact that i_{CCD} decreases with increasing Z has been extensively reported in the literature with i_{CCD} ranging from ~0.7 mA cm^{-2} to 0.05 mA cm^{-2} as Z increases from 5 Ωcm^2 to 500 Ωcm^2. Our results are broadly in this range although the predictions of i_{CCD} are on the high side compared with measurements. In Fig. 3d we show the effect of the dendrite orientation and external applied mechanical loads on i_{CCD}; see supplementary material for a detailed discussion.

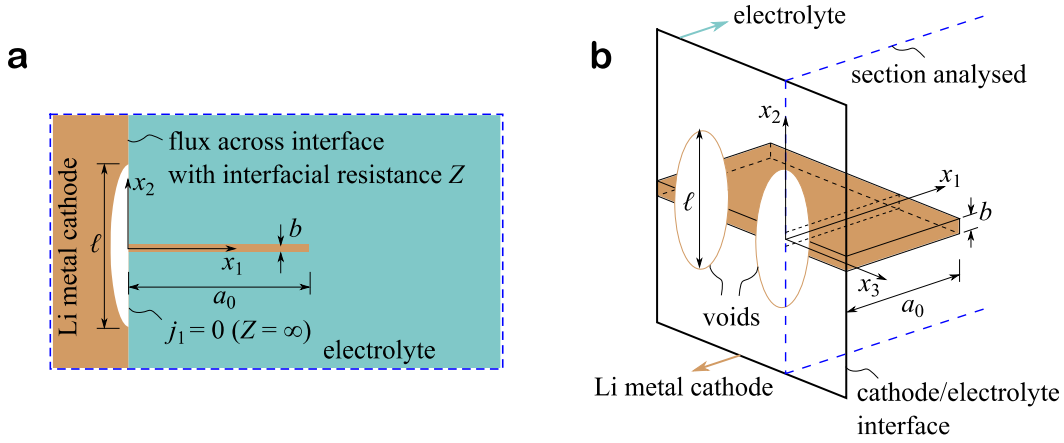

Figure 4: (a) Sketch of the 2D problem of a dendrite of length a_0 emanating at right angles from the centre of a void of size ℓ in the electrode along the electrolyte interface. The co-ordinate system (x_1, x_2) is marked and the void is modelled as patch of size ℓ with infinite ionic resistance ($Z = \infty$). (b) A 3D sketch of the void along the interface showing the electrical connection of the dendrite to the electrode. The plane indicating the section analysed in the 2D problem is also marked.

3.2 Effect of a void in the Li electrode along the cathode/electrolyte interface

Recent observations [30] have suggested that voids of size $\ell \approx 20 - 100$ μm form in the Li electrodes at the interface with the electrolyte during the consecutive plating and stripping

phases of loading of a symmetric cell. Dendrites are typically seen to grow in the vicinity of these voids, suggesting that the presence of voids enhances the driving forces for dendrite growth and here we discuss the effect of voids on i_{CCD}.

In the 2D approximation used here, we model the void of size ℓ on the cathodic interface as a patch of infinite ionic resistance ($Z = \infty$) as shown in Fig. 4a such that a zero-flux boundary ($\phi_{,i} n_i = 0$) is imposed on that region with the usual Butler-Volmer boundary conditions imposed on the remainder of the interface. A dendrite of length a_0 is assumed to emanate from the centre of the void as sketched in Fig. 4a. Of course, for this dendrite to grow by the deposition of Li^+ at its tip, it needs to be electrically connected to the cathode so as to acquire electrons and neutralize the Li^+. We envisage that this is possible in the full 3D setting as follows. While a dendrite resembles an edge dislocation forming a surface of Li in the $x_1 - x_3$ plane, discrete voids are distributed along the root of the dendrite as sketched in Fig. 4b. Thus, the Li within the dendrite is electrically connected to the cathode and the 2D analysis here is of a section as indicated in Fig. 4b and serves as an approximation of the 3D configuration depicted. However, recall that even though the dendrite is electrically connected to the cathode and thus maintained at $\phi = 0$, there is no flux of Li^+ across the dendrite flanks since the chemical potential of the Li^+ within the dendrite and the electrolyte along the flanks is equal; see the discussion around (2.16).

Before analysing the effect of the void on i_{CCD}, it is instructive to understand the effect of the void on the distribution of the electric potential and the flux of Li^+ within the dendrite. For this purpose, we consider the case where the anodic potential Φ_{P} is sufficiently low that the dendrite remains stationary and does not affect the electric field within the electrolyte in the limit $b \ll W$. The boundary conditions enforced are the Butler-Volmer conditions along the

electrode/electrolyte interfaces and no flux across the portion of the interface where the void exists along with zero flux across the dendrite flanks. There exists an intrinsic material length-scale in the problem, viz. κZ, and we shall present results here for the effect of the void size with lengths normalised by κZ. Predictions of the spatial distribution of the normalised overpotential $\bar{\eta} \equiv -(\phi + \mathcal{U})/(j_\infty Z)$ with respect to the cathode are included in Fig. 5a for a void of size $\bar{\ell} \equiv \ell/(\kappa Z) = 2.17$ and $\ell/L = 0.05$. Recall that in the absence of the void the distribution of the normalised overpotential is

$$\bar{\eta} = \left(1 + \frac{x_1}{\kappa Z}\right), \tag{3.4}$$

where $x_1 = 0$ is the cathode/electrolyte interface. The void disturbs this 1D distribution and allows high overpotentials to develop near the cathodic interface (especially towards the centre of the void) by curving the equi-overpotential lines as seen in Fig. 5a. By contrast, a concentration of the flux j_1 of Li^+ develops towards the edges of the void with the spatial distribution of the normalised flux j_1/j_∞ shown in Fig. 5b corresponding to the overpotential distribution in Fig. 5a.

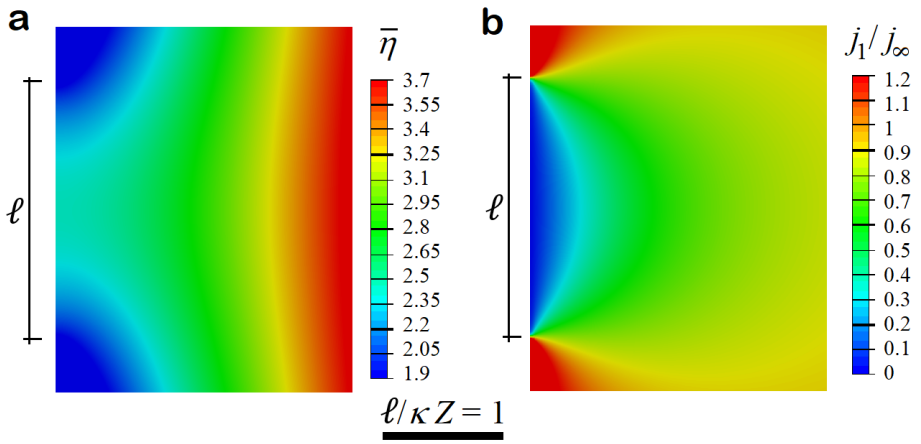

Figure 5: Numerical predictions of the spatial distribution of the normalised (a) overpotential $\bar{\eta}$ and (b) flux j_1/j_∞ in the electrolyte with an interfacial void of size $\bar{\ell} \equiv \ell/(\kappa Z) = 2.17$ and $\ell/L = 0.05$. The imposed current j_∞ is such that the dendrite remains stationary and has no effect on these fields.

To quantitatively understand the enhancement in the overpotential within the electrolyte, we plot in Fig. 6a $\bar{\eta}$ as a function of $x_1/(\kappa Z)$ along $x_2 = 0$, where the origin $(x_1, x_2) = 0$ is located at the centre of the void (Fig. 4a). Results are shown for an electrolyte of size $\ell/L = 0.05$ and selected values of $\bar{\ell}$. With increasing $\bar{\ell}$, $\bar{\eta}$ is enhanced over the no void case ($\bar{\ell} = 0$) for $x_1/(\kappa Z) < \bar{\ell}$ but the effect of the void vanishes when $x_1/(\kappa Z) \gg \bar{\ell}$. To illustrate the enhancement of $\bar{\eta}$ with increasing $\bar{\ell}$, we include in Fig. 6b the overpotential enhancement factor $k_\eta \equiv \bar{\eta}(\bar{\ell})/\bar{\eta}(\bar{\ell} = 0)$ at $(x_1, x_2) = (0,0)$ as a function of $\bar{\ell}$ for two values of ℓ/L. Clearly, k_η increases with increasing $\bar{\ell}$ and the dependence on ℓ/L is small over all reasonable values of the void to electrolyte size ratio. (We typically anticipate $\ell/L < 0.1$ given a maximum void size $\ell = 100$ μm and an electrolyte of thickness $L = 1$ mm.) It is thus reasonable to neglect the effect of ℓ/L and we proceed by presenting numerical results for $\ell/L = 0.05$.

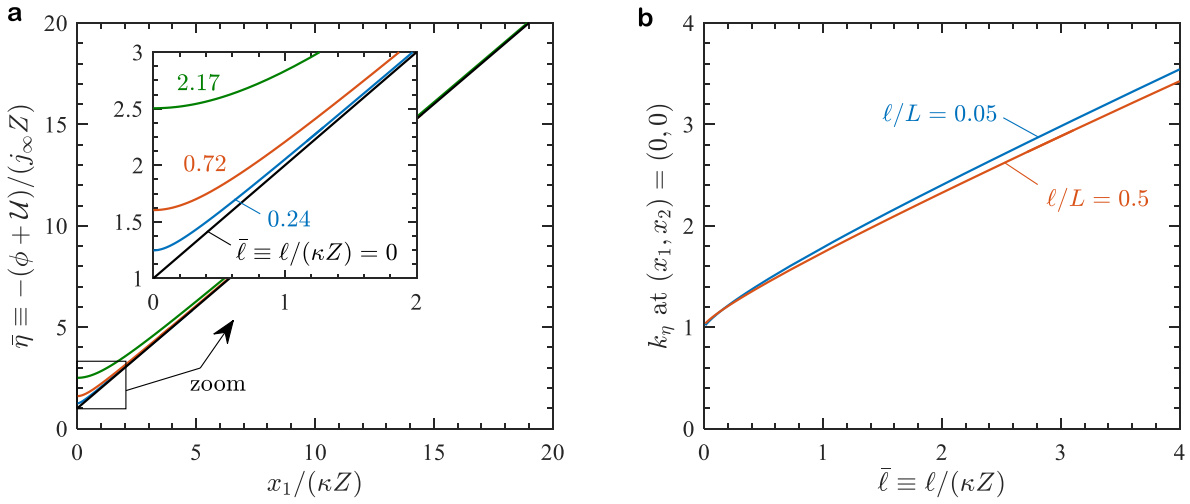

Figure 6: (a) Predictions of the variation of the normalised overpotential $\bar{\eta}$ as a function of $x_1/(\kappa Z)$ along $x_2 = 0$ for selected normalised void sizes $\bar{\ell}$ with $\ell/L = 0.05$. The co-ordinate system (x_1, x_2) is defined in Fig. 4a. (b) The overpotential concentration factor $k_\eta \equiv \bar{\eta}(\bar{\ell})/\bar{\eta}(\bar{\ell} = 0)$ at $(x_1, x_2) = (0,0)$ due to the presence of the void as a function of $\bar{\ell}$. Results are shown for two choices of ℓ/L.

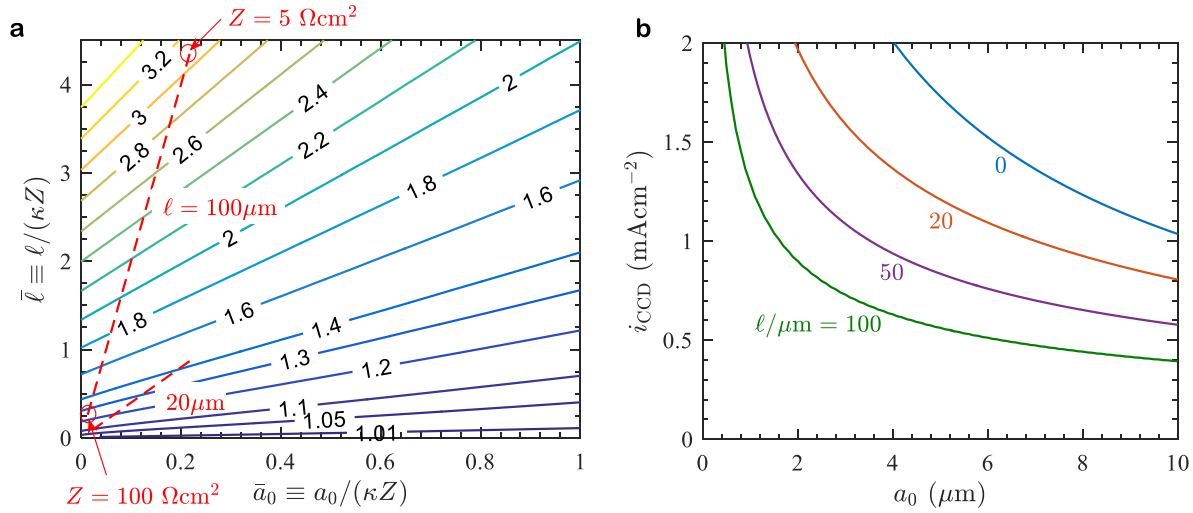

Figure 7: (a) Predictions of the overpotential concentration factor $k_{\text{tip}} \equiv \bar{\eta}(\bar{\ell}, \bar{a}_0)/\bar{\eta}(\bar{\ell} = 0, \bar{a}_0)$ at the tip of a dendrite of length a_0 due to the presence of a void of size ℓ. The numerical results are summarised via contours of k_{tip} using axes of $\bar{a}_0 \equiv a_0/(\kappa Z)$ and $\bar{\ell} \equiv \ell/(\kappa Z)$. Trajectories of increasing Z from 5 Ωcm^2 to 100 Ωcm^2 for the case of a $a_0 = 5$ μm dendrite with $\ell = 20$ μm and $\ell = 100$ μm voids are also marked by dashed lines with the left and right ends of the lines corresponding to $Z = 100$ Ωcm^2 and 5 Ωcm^2, respectively. (b) Predictions of the critical current density i_{CCD} as a function of the initial dendrite length a_0 for a cell with interfacial resistance $Z = 5$ Ωcm^2 and selected values of the void size ℓ.

Consider a dendrite inclined at $\alpha = 0^{\text{o}}$ and initial length a_0 with its root located at the centre of the void at $(x_1, x_2) = 0$. We wish to quantify the enhancement in the overpotential at the tip of the dendrite located at $(x_1, x_2) = (a_0, 0)$ due to the presence of the void. Therefore, in terms of the normalised dendrite length $\bar{a}_0 \equiv a_0/(\kappa Z)$, we define an overpotential concentration factor $k_{\text{tip}} \equiv \bar{\eta}(\bar{\ell}, \bar{a}_0)/\bar{\eta}(\bar{\ell} = 0, \bar{a}_0)$, where $\bar{\eta}(\bar{\ell}, \bar{a}_0)$ denotes the normalised overpotential at $(x_1, x_2) = (a_0, 0)$ for a void of size $\bar{\ell}$. The numerically calculated dependence of k_{tip} on $(\bar{\ell}, \bar{a}_0)$ is summarised in Fig. 7a where it is clear that k_{tip} is the highest for large $\bar{\ell}$ and small $\bar{a}_0$, i.e. for a given (κ, Z) the enhancement of the overpotential at the dendrite tip is highest for large voids and short dendrites. These numerical results can then directly be used to infer i_{CCD}

as follows. The overpotential at the dendrite tip with a void present is $\eta_{\text{tip}} = k_{\text{tip}} j_\infty (Z + a_0/\kappa)$ and substituting this into (2.36) gives an expression for $i_{\min}$ analogous to (3.2) except that the term $(Z + a_0/\kappa)$ is replaced by $k_{\text{tip}}(Z + a_0/\kappa)$. It then follows that b_{CCD} remains unaffected by the void such that

$$i_{\text{CCD}} = \frac{1}{F\rho_{\text{m}}\left(Z + \frac{a_0}{\kappa}\right)k_{\text{tip}}}\left[\frac{2\gamma_{\text{e/Li}}}{b_{\text{CCD}}} + \frac{G b_{\text{CCD}}}{4\pi(1-\nu)a_0}\right], \tag{3.5}$$

with b_{CCD} given by (3.3). In (3.5), k_{tip} is a function of $(\bar{\ell}, \bar{a}_0)$ and needs to be numerically evaluated but is succinctly summarised in the look-up chart in Fig. 7a. Predictions of i_{CCD} as a function of a_0 using this prescription are included in Fig. 7b for 4 void sizes in the range $0 \leq \ell \leq 100$ μm and an interfacial resistance $Z = 5\ \Omega\text{cm}^2$. For a given a_0, i_{CCD} decreases significantly with increasing ℓ confirming the hypothesis [30] that voids enhance the driving forces for dendrite growth.

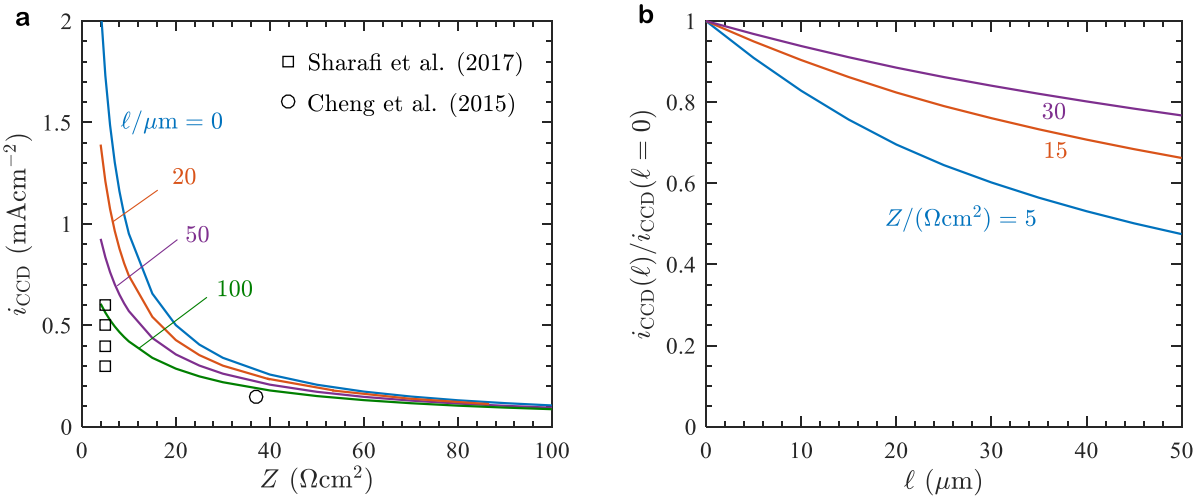

Figure 8: (a) Predictions of the critical current density i_{CCD} as a function of the interfacial resistance Z for selected values of the void size ℓ. Experimental data from Sharafi et al. [9] and Cheng et al. [31] are also included for comparison purposes. (b) The corresponding ratio $i_{\text{CCD}}(\ell)/i_{\text{CCD}}(\ell = 0)$ as a function of ℓ for three selected values of Z. All results are for a dendrite of initial length $a_0 = 5$ μm.

The interplay of Z and ℓ is investigated in Fig. 8a where we include predictions of i_{CCD} as a function of Z for selected values of ℓ and for a dendrite of length $a_0 = 5$ μm. The reduction in i_{CCD} due to the presence of the void is most pronounced at low values of Z. To understand this recall that, for a given (a_0, ℓ), increasing Z implies a decrease in $\bar{a}_0$ and $\bar{\ell}$. The trajectories of increasing Z from 5 Ωcm^2 to 100 Ωcm^2 for the case of dendrite with $a_0 = 5$ μm for voids of size $\ell = 20$ μm and $\ell = 100$ μm are marked in Fig. 7a. Clearly k_{tip} is significantly higher for the $\ell = 100$ μm case compared to the $\ell = 20$ μm case for $Z = 5$ Ωcm^2 (the top right ends of the trajectories). However, for $Z = 100$ Ωcm^2 (i.e. near the origin), the k_{tip} values for the two void sizes are approximately equal and this is directly reflected in the interplay of Z and ℓ seen in Fig. 8a. To more succinctly quantify this curious effect that a void more significantly affects i_{CCD} at lower values of Z, we include in Fig. 8b predictions of the ratio $i_{\mathrm{CCD}}(\ell)/i_{\mathrm{CCD}}(\ell = 0)$ as a function of ℓ for three selected values of Z and a dendrite of length $a_0 = 5$ μm. While $i_{\mathrm{CCD}}(\ell)/i_{\mathrm{CCD}}(\ell = 0)$ decreases with increasing ℓ, the reductions are larger at lower values of Z for a given ℓ. We emphasize that the absolute value of i_{CCD} at a given ℓ increases with decreasing Z (Fig. 8a): Fig. 8b illustrates that the detrimental effect of a void is higher at lower Z values.

Measurements of i_{CCD} reported in the literature [9, 101] as a function of the interfacial resistance are included in Fig. 8a. The measurements of Sharifi et al. [9] at $Z =$?? Show significant variability. This is attributed by Sharifi et al. [9] to a grain size effect which in our model would be reflected in terms of the length a_0 of the initial dendrite (recall the predictions in Fig. 8a are for $a_0 = 5$ μm). Nevertheless, the comparisons in Fig. 8a show good overall agreement with measurements thereby confirming the efficacy of the model.

4. Concluding remarks

The growth of dendrites from the cathodic interface is driven by the overpotential of Li^+ at the dendrite tip. The chemical potential of Li^+ within the dendrite and adjacent electrolyte equalises as Li vacancies within the dendrite are eliminated by a very small flux of Li^+. This switches-off flux of Li^+ across the dendrite flanks. In contrast, given an adequate overpotential, Li^+ can flux into the dendrite tip at constant chemical potential and drive dendrite growth. The flux at the dendrite tip is accompanied by fracture and wedging open of the electrolyte to accommodate extension of the dendrite in a dislocation-like manner, with the energy required for these processes provided by the loss of free-energy associated with the flux of Li^+ at the dendrite tip.

Since the dendrite tip overpotential is set by the current density of the cell the model predicts that dendrite growth initiates at a critical current density i_{CCD}. Predictions of i_{CCD} are in good agreement with measurements and also show that formation of defects such as voids in the electrode and the electrolyte/cathode interface reduce the critical current densities. The mechanisms which lead to the nucleation of dendrites remain a topic for future investigation although some initial studies [32] speculating on possible mechanisms have recently been reported. Nevertheless, unlike in liquid electrolytes, high-resolution observations of the morphology of dendrites in solid electrolytes has to-date not been reported in the literature and is essential to confirm the existence of the dislocation like dendrites envisioned in this study.

Acknowledgements

The authors are grateful for helpful discussions with Profs. Peter Bruce, Clare Grey and Jeff Sakamoto. NAF acknowledges support by the ERC project “Multilat” and by the Faraday Institution [Solbat, grant number FIRG007].

References

[1] J.-M. Tarascon, M. Armand *Nature* 2001, **414**, 359-367.

[2] M. Armand, J.-M. Tarascon *Nature* 2008, **451**, 652-657.

[3] L. Gireaud, S. Grugeon, S. Laruelle, B. Yriex, J.-M. Tarascon *Electrochem. Commun.* 2006, **8**, 1639-1649.

[4] K.J. Harry, D.T. Hallinan, D.Y. Parkinson, A.A. MacDowell *Nat. Mater.* 2014, **13**, 69-73.

[5] K.J. Harry, X. Liao, D.Y. Parkinson, A.M. Minor, N.P. Balsara *J. Electrochem. Soc.* 2015, **162**, A2699-A2706.

[6] C. Monroe, J. Newman *J. Electrochem. Soc.* 2004, **151**, A880-A886.

[7] C. Monroe, J. Newman *J. Electrochem. Soc.* 2005, **152**, A396-A404.

[8] A. Sharafi, E. Kazyak, A.L. Davis, S. Yu, T. Thompson, D.J. Siegel, N.P. Dasgupta, J. Sakamoto *Chem. Mater.* 2017, **29**, 7961-7968.

[9] A. Sharafi, C.G Haslam, R.D. Kerns, J. Wolfenstine, J. Sakamoto *J Mater. Chem A* 2017, **5**, 21491.

[10] A. Sharafi, H.M. Meyer, J. Nanda, J. Wolfenstine, J. Sakamoto *J. Power Sources* 2016, **302**, 135-139.

[11] R.D. Schmidt, J. Sakamoto *J. Power Sources* 2016, **324**, 126–133.

[12] B. Wu, S. Wang, J. Lochala, D. Desrochers, B. Liu, W. Zang, J. Yang, J. Xiao *Energy Environ. Sci.* 2018, **11**, 1803-1810.

[13] E.J. Cheng, A. Sharafi, J. Sakamoto *Electrochim. Acta* 2017, **223**, 85-91

[14] L.C. De Jonghe, L. Feldman, A. Beuchele *J. Mater. Sci.* 1981, **16**, 780-786.

[15] S. Zhang, K. Zhao, T. Zhu, J. Li *Prog. Mater. Sci.* 2017, **89**, 479-521.

[16] K. Zhao, M. Pharr, J.J. Vlassak, Z. Suo *J App. Phy.* 2010, **108**, 073517.

[17] L.A. Feldman, L.C. De Jonghe *J. Mater. Sci.* 1982, **17**, 517–524.

[18] L. Porz, T. Swamy, B. W. Sheldon, D. Rettenwander, T. Frömling, H.L. Thaman, S. Berendts, R. Uecker, W. C. Carter, Y.-M. Chiang *Adv. Energy Mater.* 2017, 1701003.

[19] M. Klinsmann, F.E. Hildebrand, M. Ganser, R.M. McMeeking *J. Power Sources* 2019, **422**, 227226.

[20] R.D. Armstrong, T. Dickinson, J. Turner *Electrochim. Acta* 1974, **19**, 187-192.

[21] H. Schultz, *Mater. Sci. Eng. A* 1991, **141**, 149-167.

[22] J. Newman, K.E. Thomas-Alyea *Electrochemical Systems*, 3rd Ed., Wiley 2004.

[23] A. Salvadori, D. Grazioli, M.G.D. Geers, D. Danilov, P.H.L. Notten *J. Power Sources* 2015, **293**, 892-911.

[24] E. Van der Giessen, A. Needleman *Model. Simul. Mater. Sci. Eng.* 1995, **3**, 689-735.

[25] J.P. Hirth, J. Lothe, *Theory of dislocations*, 2nd Ed., McGraw-Hill 1982.

[26] C. Ayas, J.A.W. van Dommelen, V.S. Deshpande *J. Mech. Phys. Solids* 2014, **62**, 113-136.

[27] R.F. Bishop, R. Hill, N.F. Mott, *Proc. Phys. Soc.* 1945, **57**, 147-159.

[28] D. Rettenwander, A. Welzl, L. Cheng, J. Fleig, M. Musso, E. Suard, M.M. Doeff, G.J. Redhammer, G. Amthauer *Inorg. Chem.* 2015, **54**, 10440–10449.

[29] J.E. Ni, E.D. Case, J. Sakamoto, E. Rangasamy, J. Wolfenstine *J. Mater. Sci.* 2012, **47**, 7978-7985.

[30] J. Kasemchainan, S. Zekoll1, D.S. Jolly, Z. Ning, G.O. Hartley, J. Marrow, P.G. Bruce *Nat. Mater.* 2019, https://doi.org/10.1038/s41563-019-0438.

[31] L. Cheng, W. Chen, M. Kunz, K. Persson, N. Tamura, G. Chen, M. Doeff *ACS App. Mater. Interfaces* 2015, **7**, 2073-2081.

[32] G. Li, C. Monroe *Phys. Chem. Chem. Phys.* 2019, **21**, 20354.

SUPPLEMENTARY MATERIAL

Dendrites as climbing dislocations in ceramic electrolytes: initiation of growth

S. S. Shishvan[a,b], N.A. Fleck[b], R.M. McMeeking[c,d,e] and V.S. Deshpande[b*]

[a] *Department of Structural Engineering, University of Tabriz, Tabriz, Iran*

[b] *Department of Engineering, University of Cambridge, Cambridge CB2 1PZ, UK*

[c] *Department of Mechanical Engineering & Materials Department, University of California, Santa Barbara CA 93106, USA*

[d] *School of Engineering, Aberdeen University, King's College, Aberdeen AB24 3UE, UK*

[e] *INM – Leibniz Institute for New Materials, Campus D2 2, 66123 Saarbrücken, Germany*

Contents:

A. Derivation of the Butler-Volmer interface kinetic relation

Here, we provide a derivation of the Butler-Volmer kinetics between the electroneutral single ion-conductor electrolyte and a Li metal electrode to not only include the effects of pressure in the electrode but also clarify some of the key assumptions. An understanding of these assumptions will illuminate the differences in the kinetics between the electrolyte/electrodes interfaces and electrolyte/dendrite interfaces.

In order to derive an interface kinetic law, we interpret the molar densities $N^{\mathrm{e}}_{\mathrm{Li}^+}$, $N^{\mathrm{e}}_{\mathrm{L}}$, $N^{\mathrm{m}}_{\mathrm{Li}^+}$ and $N^{\mathrm{m}}_{\mathrm{L}}$ as areal densities over the interface in the electrolyte and Li electrode with θ_{m} and θ^0_{e} the corresponding surface occupancies of sites by Li^+ in the electrode and electrolyte, respectively. The chemical potentials of the Li^+ in the electrode and electrolyte are given by (2.11) and (2.12), respectively, and we define the standard chemical potentials $\chi^{\mathrm{m}}_{\mathrm{Li}^+}$ and $\chi^{\mathrm{e}}_{\mathrm{Li}^+}$ of Li^+ in the electrode and electrolyte, respectively, as

$$\chi^{\mathrm{m}}_{\mathrm{Li}^+} \equiv (\mu^0_{\mathrm{m}} - h_{\mathrm{v}}) + F\phi_{\mathrm{m}} + p_{\mathrm{m}}(\Omega_{\mathrm{Li}} - \Omega_{\mathrm{v}}), \tag{A1}$$

and

$$\chi^{\mathrm{e}}_{\mathrm{Li}^+} \equiv \mu^0_{\mathrm{e}} + F\phi_{\mathrm{e}}, \tag{A2}$$

which are the chemical potentials absent the configurational entropy. First, consider the rate of flux of Li^+ from electrode to electrolyte. With ω denoting the jump frequency of Li^+ ions and χ_a the activation barrier, this forward reaction rate is

$$r_+ = \underbrace{\omega N^{\mathrm{m}}_{\mathrm{Li}^+}\theta_{\mathrm{m}}}_{\text{(a)}} \underbrace{\exp\left[-\frac{(\chi_a - \chi^{\mathrm{m}}_{\mathrm{Li}^+})}{RT}\right]}_{\text{(b)}} \underbrace{\frac{N^{\mathrm{e}}_{\mathrm{Li}^+}(1-\theta^0_{\mathrm{e}})}{N^{\mathrm{e}}_{\mathrm{Li}^+} + N^{\mathrm{m}}_{\mathrm{Li}^+}}}_{\text{(c)}}, \tag{A3}$$

where (a) is the number of attempts per unit time, (b) is the probability that an attempt is successful in crossing the activation barrier and (c) is the probability that the Li^+ ion that

successfully crosses the barrier finds an empty electrolyte site. Similarly, the flux rate of Li^+ from the electrolyte to electrode (i.e. backward reaction rate) is

$$r_- = \omega N^{\mathrm{e}}_{\mathrm{Li}^+}\theta^0_{\mathrm{e}}\ \exp\left[-\frac{(\chi_a - \chi^{\mathrm{e}}_{\mathrm{Li}^+})}{RT}\right]\frac{N^{\mathrm{m}}_{\mathrm{Li}^+}(1-\theta_{\mathrm{m}})}{N^{\mathrm{e}}_{\mathrm{Li}^+}+N^{\mathrm{m}}_{\mathrm{Li}^+}}, \tag{A4}$$

so that the net current from the electrode to electrolyte is given by $j = F(r_+ - r_-)$. The key constitutive assumption in Butler-Volmer kinetics is that the activation barrier is at a height χ^0_a above the weighted mean of the standard chemical potentials of the two end-states, i.e.

$$\chi_a = \chi^0_a + \left[\beta\chi^{\mathrm{m}}_{\mathrm{Li}^+} + (1-\beta)\chi^{\mathrm{e}}_{\mathrm{Li}^+}\right], \tag{A5}$$

where β is the Butler-Volmer symmetry factor and satisfies $0 \le \beta \le 1$. Substituting (A5) into (A3) and (A4) and employing the definition $\eta \equiv (\phi_{\mathrm{m}} - \phi_{\mathrm{e}}) - \mathcal{U}$ along with the relation (2.13) for the open circuit potential $\mathcal{U}$, we have

$$j = q_0\left\{\theta_{\mathrm{m}}\exp\left[\frac{(1-\beta)F\eta - h_{\mathrm{v}}}{RT}\right] - (1-\theta_{\mathrm{m}})\exp\left[\frac{-\beta F\eta - p_{\mathrm{m}}(\Omega_{\mathrm{Li}}-\Omega_{\mathrm{v}})}{RT}\right]\right\}, \tag{A6}$$

where

$$q_0 = \frac{\omega F N^{\mathrm{e}}_{\mathrm{Li}^+}N^{\mathrm{m}}_{\mathrm{Li}^+}}{N^{\mathrm{e}}_{\mathrm{Li}^+}+N^{\mathrm{m}}_{\mathrm{Li}^+}}\exp\left(-\frac{\chi^0_a}{RT}\right)\exp\left[\frac{(1-\beta)p_{\mathrm{m}}(\Omega_{\mathrm{Li}}-\Omega_{\mathrm{v}})+\beta h_{\mathrm{v}}}{RT}\right]\theta^0_{\mathrm{e}}\left(\frac{\theta^0_{\mathrm{e}}}{1-\theta^0_{\mathrm{e}}}\right)^{-\beta}. \tag{A7}$$

Setting $p_{\mathrm{m}} = p$ and $j = 0$ in (A6), we recover the equilibrium relation (2.16) for the occupancy of the Li sites within the dendrite, i.e. the occupancy of Li sites within the dendrites to switch off flux from the electrolyte into the dendrite. This occupancy is also given by equating the chemical potentials of Li^+ in the electrolyte and dendrite as discussed in the main text.

Flux across the electrode/electrolyte interface differs from that at the dendrite/electrolyte interface in the sense that it is assumed that the electrode is maintained in equilibrium with a vacancy reservoir. This directly sets θ_{m} via (2.6) and keeps the Li^+ in the electrode out of equilibrium with the Li^+ in the adjacent electrolyte resulting in a continued flux. This flux is obtained by substituting (2.6) and using (2.7) to reduce (A6) to

$$j = q_0(1-\theta_{\mathrm{m}})\left\{\exp\left[\frac{(1-\beta)F\eta + p_{\mathrm{m}}\Omega_{\mathrm{v}}}{RT}\right] - \exp\left[\frac{-\beta F\eta - p_{\mathrm{m}}(\Omega_{\mathrm{Li}} - \Omega_{\mathrm{v}})}{RT}\right]\right\}, \qquad \text{(A8)}$$

which can be recast as Eqs. (2.14) and (2.15) with the reference exchange current given by

$$\bar{J}_0 = \frac{\omega F N^{\mathrm{e}}_{\mathrm{Li}^+} N^{\mathrm{m}}_{\mathrm{Li}^+}}{N^{\mathrm{e}}_{\mathrm{Li}^+} + N^{\mathrm{m}}_{\mathrm{Li}^+}} \exp\left(-\frac{\chi^0_a}{RT}\right)\left(\frac{1-\theta^0_{\mathrm{m}}}{\theta^0_{\mathrm{m}}}\frac{\theta^0_{\mathrm{e}}}{1-\theta^0_{\mathrm{e}}}\right)^{-\beta} \theta^0_{\mathrm{e}}(1-\theta^0_{\mathrm{m}}). \qquad \text{(A9)}$$

In (A9), θ^0_{m} is related to the enthalpy of vacancy formation h_{v} in Li via Eq. (2.7).

B. Discussion on boundary conditions to Laplace's equation

The boundary conditions imposed on the Laplace equation (2.17) require some clarification with regard satisfying Gauss's law and the Maxwell-Faraday equation along the interfaces.

First consider the Robin-type boundary conditions along electrolyte/electrode interfaces resulting from the Butler-Volmer flux law. The solution of the boundary value problem furnishes $\phi_{,i}n_i$ at the interfaces, where n_i is the unit outward normal to the electrolyte. The electric field within the electrode vanishes and thus Gauss's law requires that an areal density of charge (bound plus free charge) $q = \mathcal{E}_0\phi_{,i}n_i$ develops over these interfaces, where $\mathcal{E}_0$ is the permittivity of free-space. By contrast, we have a zero-flux Neumann boundary condition across the electrolyte/dendrite interface with $\phi_{,i}n_i = 0$. The electric field vanishes within the dendrite and hence Gauss's law requires $q = 0$ over that interface. Finally, consider the electrolyte/free-space interface. Again, we impose the zero-flux condition $\phi_{,i}n_i = 0$ along that interface. However, an electric field can develop in free-space (e.g. fringing effect in a capacitor) and thus a direct application of Gauss's law does not provide q. Rather we argue that since the electrolyte remains electroneutral and no charge on the interface can be generated from free-space, $q = 0$. Thus, Gauss's law requires that the normal component of the electric field within free-space along those interfaces also vanishes.

While the above discussion demonstrates that Gauss's law is satisfied along these interfaces, now consider the Maxwell-Faraday equation: in an electrostatic situation, it reduces to $\mathrm{curl}(E_i) = 0$. The fact that we have defined $E_i \equiv -\phi_{,i}$ ensures that the Maxwell-Faraday equation is automatically satisfied within the electrolyte but jumps in ϕ across interfaces need special attention. Across an interface, $\mathrm{curl}(E_i) = 0$ implies that the tangential component of the electric field $\phi_{,i}s_i$ is continuous, where s_i is a unit vector along the interface. Let us first consider the electrolyte/electrode interfaces. Along these interfaces, the boundary condition to Laplace's equation is the Robin-type Butler-Volmer boundary condition which couples together the electric potential jump across the interface and the normal electric field $\phi_{,i}n_i$ within the electrolyte. With the electric field vanishing in the electrode, we require $\phi_{,i}s_i = 0$ in the electrolyte along these interfaces but we have no direct control over $\phi_{,i}s_i$. It is thus clear that we might be in violation of the Maxwell-Faraday equation along the electrode/electrolyte interfaces. To resolve this issue, we hypothesize that an interlayer of thickness h develops along these interfaces as sketched in Fig. 2. To understand the governing equations within this interlayer we denote the electric potential within the interlayer at a location (x, y) by $\psi(x, y)$ and $h(x)$ the thickness of the interlayer at a location x along the electrolyte (the co-ordinate system (x, y) is defined in the insets of Fig. 2). The potential $\psi(x, h(x)) = 0$ and $\psi(x, 0) = \phi(x)$, where $\phi(x)$ is the potential of the electrolyte along the electrolyte/electrode interface. These boundary conditions ensure continuity of potentials along the interlayer/electrolyte and interlayer/electrode interfaces. With the electric field within the interlayer given by $E_i = -\psi_{,i}$, the Maxwell-Faraday equation is automatically satisfied. Now consider Gauss's law within the interlayer which reads

$$\varepsilon_0 \psi_{,ii} = -\rho, \tag{B1}$$

where the total charge (bound plus free) density ρ within the interlayer is related to the surface charge via

$$q(x) = \int_0^{h(x)} \rho(x,y)dy, \tag{B2}$$

where $q = \mathcal{E}_0 \phi_{,i} n_i$ is the areal surface charge derived from the normal electric field in the electrolyte at the electrolyte/electrode interface. Of course, Eqs. (B1) and (B2) are insufficient to solve the fields within the interlayer and additional constitutive understanding is required to complete the specification. However, these equations demonstrate that all the required electrostatic governing equations can be satisfied by the existence of such an interlayer. In the main paper, we do not need a complete understanding of the interlayer. Rather, we just require that the thickness of the interlayer is small compared to other leading dimensions[iv] and that the flux across the interlayer is directly given by the Butler-Volmer equation with the exchange current setting the resistance for Li^+ to cross this interlayer. The situation is identical for the interlayer along the electrolyte/dendrite interface except that (B2) is modified to

$$\int_0^{h(x)} \rho(x,y)dy = 0, \tag{B3}$$

as no surface charge is generated along these interfaces.

Finally, consider the electrolyte/free-space interface. The solution of Laplace's equation (2.17) with the Neumann zero-flux boundary condition furnishes the tangential electric field $\phi_{,i} s_i$ in the electrolyte along these interfaces. To ensure that the Maxwell-Faraday equation is satisfied, an equal tangential electric field is induced in free-space as, unlike the metallic Li, free-space can sustain a finite electric field. (Recall that Gauss's law requires that the normal component of the electric field vanishes in free-space along these interfaces as discussed above.) Thus, no interlayer is required along these interfaces to ensure that the electrostatic governing equations

[iv] The interlayer is expected to scale with the Debye length and hence on sub nanometer length scale implying that this condition is easily satisfied.

hold. The resulting electric field in free space along the electrolyte/free space interface, upon integration along the interface, provides Dirichlet boundary conditions of electric potential for solution of Laplace's equation in free space to determine the fringing field around the symmetric cell. Such boundary conditions need to be augmented in free space along the free outer surfaces of the electrodes, e.g. Dirichlet boundary conditions set by the electrode voltages. While there is no need to compute the resulting fringing field for the purposes of the analysis presented here, it is relevant that it can be done without violating the Maxwell-Faraday condition.

C. The elastic fields of an edge dislocation in a half-space

We consider an edge dislocation in an elastic half space with shear modulus G and Poisson's ratio ν and a traction-free surface along $y = 0$ as sketched in Fig. S1. The dislocation is located at a distance h from the free-surface and with a Burgers vector of magnitude b making an angle α with the free-surface. This dislocation thus represents a dendrite of length $a_0 = h/\cos\alpha$.

The stress field σ_{ij} of this dislocation is given by the sum of the singular stress field $\tilde{\sigma}_{ij}$ of this edge dislocation in an infinite medium and a non-singular image field $\hat{\sigma}_{ij}$ that corrects for the traction free-boundary along $y = 0$, i.e. $\sigma_{ij} = \tilde{\sigma}_{ij} + \hat{\sigma}_{ij}$ [1]. The field $\tilde{\sigma}_{ij}$ is known trivially and given by [2]

$$\begin{aligned}
\tilde{\sigma}_{xx} &= \frac{-G}{2\pi(1-\nu)}\left[b_x \frac{(y-h)(3x^2+(y-h)^2)}{(x^2+(y-h)^2)^2} + b_y \frac{x((y-h)^2-x^2)}{(x^2+(y-h)^2)^2}\right], \\
\tilde{\sigma}_{yy} &= \frac{G}{2\pi(1-\nu)}\left[b_x \frac{(y-h)(x^2-(y-h)^2)}{(x^2+(y-h)^2)^2} + b_y \frac{x(3(y-h)^2+x^2)}{(x^2+(y-h)^2)^2}\right], \\
\tilde{\sigma}_{xy} &= \frac{G}{2\pi(1-\nu)}\left[b_x \frac{x(x^2-(y-h)^2)}{(x^2+(y-h)^2)^2} - b_y \frac{(y-h)((y-h)^2-x^2)}{(x^2+(y-h)^2)^2}\right],
\end{aligned} \tag{C1}$$

where $b_x = -b\cos\alpha$ and $b_y = b\sin\alpha$. The total solution with the $\hat{\sigma}_{ij}$ field correcting for the boundary condition is more complicated and an analytical solution was developed by Freund

[3] using the complex stress function approach. The solution can be expressed in terms of a single complex analytic function φ of $\zeta = x + \imath y$, where $\imath \equiv \sqrt{-1}$ with σ_{ij} given by

$$\begin{aligned} \sigma_{yy} - \imath\sigma_{xy} &= \varphi'(\zeta) - \varphi'(\bar{\zeta}) + (\zeta - \bar{\zeta})\overline{\varphi''(\zeta)}, \\ \sigma_{xx} + \imath\sigma_{xy} &= \varphi'(\zeta) - \varphi'(\bar{\zeta}) + 2\overline{\varphi'(\zeta)} - (\zeta - \bar{\zeta})\overline{\varphi''(\zeta)}, \end{aligned} \tag{C2}$$

where overbar denotes the complex conjugate and

$$\begin{aligned} \varphi'(\zeta) &= \frac{-G}{4\pi(1-\nu)}\left[\frac{\imath\left(b_x + \imath b_y\right)}{\zeta - \imath h} - \frac{\imath\left(b_x - \imath b_y\right)(\zeta - \imath h)}{(\zeta + \imath h)^2} - \frac{\imath\left\{\left(b_x + \imath b_y\right) - \left(b_x - \imath b_y\right)\right\}}{\zeta + \imath h}\right], \\ \varphi''(\zeta) &= \frac{-G}{\pi(1-\nu)}\left[\frac{\left(b_x + \imath b_y\right)\zeta h}{(\zeta^2 + h^2)^2} + \frac{\left(b_x - \imath b_y\right)h}{(\zeta + \imath h)^3}\right]. \end{aligned} \tag{C3}$$

By subtracting the stress field (C1) from the fields given in (C2), we obtain the image stress field at the location of dislocation as

$$\begin{aligned} \hat{\sigma}_{xx}^{\text{tip}}(x = 0, y = h) &\equiv \lim_{\substack{x\to 0 \\ y\to h}}[\sigma_{xx}(x,y) - \tilde{\sigma}_{xx}(x,y)] = \frac{-Gb\cos\alpha}{4\pi(1-\nu)h}, \\ \hat{\sigma}_{yy}^{\text{tip}}(x = 0, y = h) &\equiv \lim_{\substack{x\to 0 \\ y\to h}}\left[\sigma_{yy}(x,y) - \tilde{\sigma}_{yy}(x,y)\right] = \frac{Gb\cos\alpha}{4\pi(1-\nu)h}, \\ \hat{\sigma}_{xy}^{\text{tip}}(x = 0, y = h) &\equiv \lim_{\substack{x\to 0 \\ y\to h}}\left[\sigma_{xy}(x,y) - \tilde{\sigma}_{xy}(x,y)\right] = \frac{Gb\sin\alpha}{4\pi(1-\nu)h}. \end{aligned} \tag{C4}$$

The climb component of the Peach-Koehler force is $f_{\text{climb}} \equiv -\hat{\sigma}_{ij}^{\text{tip}} m_i m_j b$, where $m_i \equiv (-\cos\alpha, \sin\alpha)$, i.e.

$$f_{\text{climb}} = -b\left[\hat{\sigma}_{xx}^{\text{tip}}\cos^2\alpha + \hat{\sigma}_{yy}^{\text{tip}}\sin^2\alpha - \hat{\sigma}_{xy}^{\text{tip}}\sin 2\alpha\right]. \tag{C5}$$

Upon substituting from (C4), we get

$$f_{\text{climb}} = \frac{Gb^2\cos\alpha}{4\pi(1-\nu)h} = \frac{Gb^2}{4\pi(1-\nu)a_0}, \tag{C6}$$

and we observe that f_{climb} expressed in terms of the dendrite length a_0 is independent of the inclination α.

Finally, it is worth understanding the pressure $p_{\text{tip}} \equiv -\sigma_{kk}/3$ at the dendrite tip. The image contribution follows from (C4) as

$$\hat{p}_{\text{tip}} \equiv -\frac{(1+\nu)\left(\hat{\sigma}_{xx}^{\text{tip}} + \hat{\sigma}_{yy}^{\text{tip}}\right)}{3} = 0. \tag{C7}$$

The singular infinite medium field $\tilde{\sigma}_{ij}$ is undefined at the location of dislocation (i.e. dendrite tip) but it is instructive to consider the limit as we approach the tip. It is convenient to rewrite (C1) in polar co-ordinates as

$$\tilde{\sigma}_{rr}(r,\theta) = \tilde{\sigma}_{\theta\theta}(r,\theta) = -\frac{Gb\sin\theta}{2\pi(1-\nu)r}, \tag{C8}$$

and a corresponding $\tilde{\sigma}_{r\theta}$ that is not relevant to this discussion. Here, r is the radial distance of the material point at which the stress is being calculated from the location of dislocation (i.e. dendrite tip) and θ the angle of that point with respect to the Burgers vector. Then, we define $\tilde{p}_{\text{tip}}$ as

$$\tilde{p}_{\text{tip}} \equiv \left[\frac{1}{2\pi r}\int_0^{2\pi} -\frac{(1+\nu)}{3}(\tilde{\sigma}_{rr} + \tilde{\sigma}_{\theta\theta}) r \, d\theta\right]_{r=0^+}. \tag{C9}$$

Substituting from (C8), it follows that $\tilde{p}_{\text{tip}} = 0$ and hence there is no contribution to the dendrite tip pressure from the singular infinite medium field of the dislocation. Thus, with no contribution to the pressure from the dislocation self-stress fields, the pressure at the dendrite tip is purely due to the external applied tractions as expressed in the main text immediately after (2.23).

D. Choice of parameters related to interfacial ionic resistance

Table 2 in the main text does not include the exchange current $\bar{\jmath}_0$, the symmetry factor β and the open circuit potential $\mathcal{U}$ which remain to be specified. Linearization assuming $F\eta/(RT) \ll 1$ reduces the Butler-Volmer relation (2.14) to $j = \bar{\jmath}_0 F\eta/(RT)$ with $p_{\text{m}} = 0$. Experimental measurements [4, 5] typically report a relationship between the current and overpotential across

the electrode/electrolyte interface as $j = \eta/Z$, where Z is the interfacial resistance. Comparing this to the linearized Butler-Volmer relation, it follows that $\bar{j}_0 = RT/(ZF)$ and we report predictions in terms of Z. Surface treatments and other processing routes affect Z substantially with values in the literature reported in the range $3\ \Omega\text{cm}^2 < Z < 500\ \Omega\text{cm}^2$ and we present results over approximately this range. In the linearized limit, β does not play a role but β is required for the fully non-linear Butler-Volmer relation. Here, in line with the majority of the literature, we set $\beta = 1/2$ although, as shall be seen subsequently, all results are adequately approximated by the linearized version of (2.14) implying that β plays no role in the numerical results. Direct measurements of $\mathcal{U}$ in the literature are sketchy. However, for the symmetric Li/LLZO/Li cell where we assume that $\mathcal{U}$ is the same between the electrolyte/electrodes interfaces and electrolyte/dendrite interfaces, the overpotential within the electrolyte for a given applied current density is independent of $\mathcal{U}$. The majority of the results are presented in terms of the imposed current and in the few cases where voltages are discussed we shall normalise the results so as to remove explicit dependence of the results on $\mathcal{U}$.

E. Effect of external applied loads and the dendrite angle

External applied compressive loads are expected to inhibit dendrite growth with the most potent effect resulting from external applied stresses Σ_{22} with $\Sigma_{11} = 0$ (see Fig. 1). The effect of these stresses is to enhance the elastic work required to wedge open the electrolyte as parameterised by f_{climb}; see Eq. (2.23). Given that the approximate analysis where we assume $\theta_{\text{tip}} \approx 1$ gives results to a very high level of accuracy, here we present results using such an analysis for a dendrite of length a_0 and emanating from the cathode at an angle α (Fig. 1).

Following an analysis in lines with that of presented in Section 3.1, we have

$$i_{\min} \approx \frac{1}{F\rho_{\mathrm{m}}\left(Z+\frac{a_0}{\kappa}\right)}\left[\frac{2\gamma_{\mathrm{e/Li}}}{b}+\frac{Gb}{4\pi(1-\nu)a_0}-\Sigma_{22}\cos^2\alpha\right], \tag{E.1}$$

and thus the magnitude of the Burgers vector b_{CCD} that minimizes $i_{\min}$ is independent of Σ_{22} and α and given by (3.3). Predictions of $i_{\mathrm{CCD}} = i_{\min}(b = b_{\mathrm{CCD}})$ are included in Fig. 3d as a function of Σ_{22} for a dendrite of length $a_0 = 5$ μm and $Z = 5\ \Omega\mathrm{cm}^2$ (all other parameters are fixed at their reference values and a perfect cathodic interface with no void is assumed). The critical current density i_{CCD} increases with increasing compressive stress Σ_{22} with the effect being most significant for a dendrite that emanates normally ($\alpha = 0^{\mathrm{o}}$) from the cathodic interface. In fact, i_{CCD} is independent of α for $\Sigma_{22} = 0$. Nevertheless, the enhancement in i_{CCD} is a maximum of about 7% at $\Sigma_{22} = -5$ MPa over the case when no external mechanical loads are applied.

Supplementary References

[1] E. Van der Giessen, A. Needleman *Model. Simul. Mater. Sci. Eng.* 1995, **3**, 689-735.

[2] J.P. Hirth, J. Lothe *Theory of dislocations*, McGraw-Hill 1968.

[3] L.B. Freund *Adv. App. Mech.* 1994, **30**, 1-66.

[4] A. Sharafi, E. Kazyak, A.L. Davis, S. Yu, T. Thompson, D.J. Siegel, N.P. Dasgupta, J. Sakamoto *Chem. Mater.* 2017, **29**, 7961-7968.

[5] A. Sharafi, C.G Haslam, R.D. Kerns, J. Wolfenstine, J. Sakamoto *J Mater. Chem A* 2017, **5**, 21491.

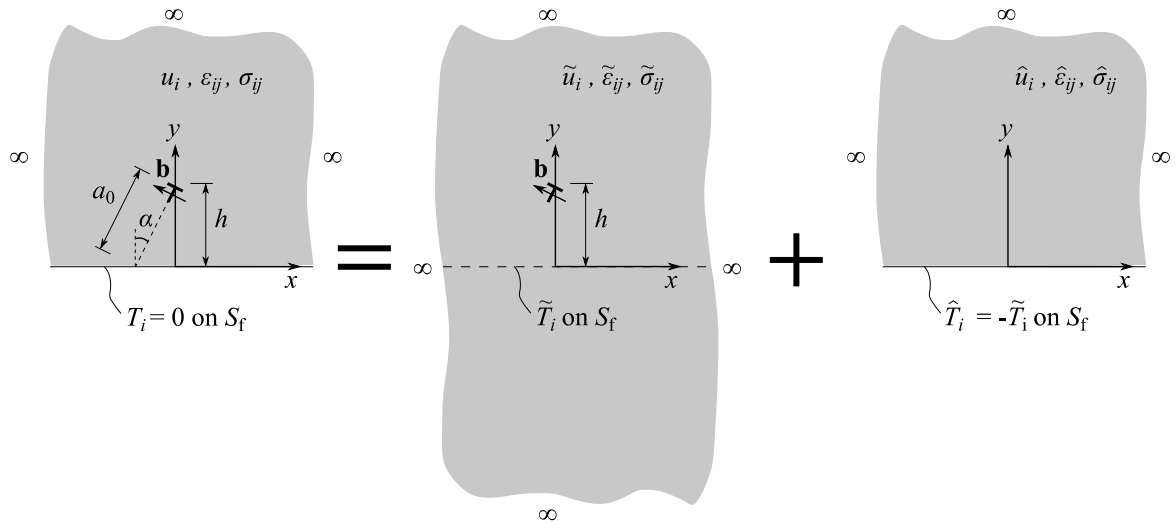

Figure S1: A sketch showing the ($\widetilde{}$) and ($\widehat{}$) problems whose superposition gives the elastic solution for an edge dislocation with Burgers vector $\boldsymbol{b}$ in a half-space with a traction-free surface along $y = 0$.